Ore Geology Reviews 87 (2017) 41–61

Contents lists available at ScienceDirect

Ore Geology Reviews

journal homepage: www.elsevier.com/locate/oregeorev

Strategic and rare elements in Cretaceous-Cenozoic cobalt-rich ferromanganese crusts from seamounts in the Canary Island Seamount Province (northeastern tropical Atlantic)

E. Marino [a,b,c,*], F.J. González [a], L. Somoza [a], R. Lunar [b,c], L. Ortega [b], J.T. Vázquez [d], J. Reyes [a], E. Bellido [a]

[a] Geological Survey of Spain, (IGME), C/Ríos Rosas, 23, 28003 Madrid, Spain
[b] Crystallography and Mineralogy Department, Complutense University of Madrid, C/Jose Antonio Novais, 2, 28040 Madrid, Spain
[c] Instituto de Geociencias IGEO (CSIC, UCM), Madrid, Spain
[d] Instituto Español de Oceanografía, C.O. de Málaga, Puerto Pesquero s/n, 29649 Fuengirola, Spain

ARTICLE INFO

Article history:
Received 1 April 2016
Received in revised form 20 September 2016
Accepted 7 October 2016
Available online 13 October 2016

Keywords:
Ferromanganese crusts
Atlantic Ocean
Phosphatization
Strategic metals
Cretaceous seamounts
Co-chronometer

ABSTRACT

Thick ferromanganese (Fe-Mn) crusts from four Cretaceous seamounts (The Paps, Tropic, Echo and Drago) at the southern Canary Island Seamount Province (CISP) in the northeastern tropical Atlantic were recovered along the flanks and summits from 1700 to 3000 m water depths. CISP is composed of >100 seamounts and submarine hills, is likely the oldest hotspot track in the Atlantic Ocean, and is the most long-lived of known hotspots globally. The Fe-Mn crusts grow on basalt-sedimentary rock substrates below the northeastern tropical Atlantic core of the oxygen minimum zone (OMZ) with a maximum thickness of 250 mm at a water depth of 2400 m. The mineralogical and chemical composition of these Fe-Mn crusts indicate a hydrogenetic origin. The main Mn minerals are vernadite with minor interlayered todorokite and asbolane-buserite. Fe oxides are essentially ferroxyhyte and goethite. The Fe-Mn crusts show high average contents in Fe (23.5 wt%), Mn (16.1 wt%), and trace elements like Co (4700 μg/g), Ni (2800 μg/g), V (2400 μg/g) and Pb (1600 μg/g). Rare earth elements plus yttrium (REY) averages 2800 μg/g with high proportions of Ce (1600 μg/g). Total platinum group elements (PGEs) average 230 ng/g, with average Pt of 182 ng/g. Two main types of growth layers form the crusts: 1) a dense laminae of oxides with high contents in Mn, Co and Ni associated with vernadite and Cu, Ni, and Zn associated with todorokite; 2) botryoidal layers with high contents in Fe, Ti, V and REY associated with goethite. The Fe-Mn crusts from the CISP region show higher contents in Fe, V, Pb and REY but lower Mn, Co, Ni and PGEs contents than Pacific or Indian ocean seamount crusts. The oldest maximum age of initiation of crust growth was at 76 Ma (Campanian, Late Cretaceous). Using a combination of high resolution Co-chronometer and geochemical data along an Electron Probe Micro Analysis (EPMA) transect, four stages in morphology, chemical contents and growth rates can be differentiated in the the Cenozoic crusts since 28 Ma, which we interpret as due to changes in the ventilation of the North Atlantic OMZ and to the increase of Saharian dust inputs. An earliest growth period, characterized by similar contents of Fe and Mn in the interval 27.8–24.45 Ma (late Oligocene-early Miocene) reflects slow precipitation related to a thick OMZ. An intermediate laminated zone with higher contents of Fe, Si and P, high growth rates reaching 4.5 mm/Ma, and precipitation of Fe-Mn oxides during the interval 24.5–16 Ma is related to periods of ventilation of the OMZ by intrusion of deep upwelling currents. Significant increase in Fe contents at ca. 16 Ma correlates with the onset of incursions of Northern Component Waters into the North Atlantic. Finally, since 12 Ma, the very low growth rates (<0.5 mm/Ma) of the crust are related to a thick North Atlantic OMZ, an increase in Sahara dust input and a stable thermohaline circulation.

1. Introduction

Ferromanganese (Fe-Mn) crusts occur globally throughout the ocean and on seamounts, ridges and plateaus where currents have kept the rocks swept clean of sediments for millions of years (e.g., Koschinsky et al., 1996; Hein et al., 1997, 2000, 2013; Rona, 2008). The first Fe-Mn crusts were collected southwest of the Canary Islands on HMS Challenger cruises in the late nineteenth century (Murray and Renard, 1891). Crusts form at water depths of about 400–7000 m, the thickest ones occurring at depths of about 800–2500 m (Hein and Koschinsky, 2014). Fe-Mn crusts have been systematically studied since the 1980s (Halbach et al., 1981; Baturin, 1988;

* Corresponding author at: Geological Survey of Spain, C/Ríos Rosas, 23, 28003 Madrid, Spain.
E-mail address: emarino@ucm.es (E. Marino).

http://dx.doi.org/10.1016/j.oregeorev.2016.10.005
0169-1368/

Bogdanov et al., 1995; Hein et al., 1997). These Fe-Mn crusts are enriched in base metals and strategic and critical elements such as Co, V, Ni, Ti, platinum group elements (PGEs) or rare earth elements (REEs) plus yttrium (REY) and are being considered for future mining (Baturin, 1988; Hein et al., 1997, 2013; González et al., 2012).

According to the International Seabed Authority (ISBA, 2016), 'cobalt crusts' are defined as hydroxide/oxide deposits of cobalt-rich iron/manganese (ferromanganese) crusts formed by direct precipitation of minerals from seawater onto hard substrates, containing minor but significant concentrations of Co, Ti, Ni, Pt, Mo, Te, Ce, other metallic and REEs (ISBA/16/C/WP2). Four main types of Fe-Mn deposits have been traditionally recognized (Hein et al., 2000): Hydrogenetic crusts, hydrogenetic-diagenetic nodules, mixed hydrothermal-hydrogenetic crusts, and stratabound hydrothermal deposits. Mixed hydrogenetic-diagenetic Fe-Mn pavements and nodules related to the oxidation of metals in hydrocarbon seeps occur in the Gulf of Cádiz (González et al., 2012).

At present, the strategic elements of interest for future mining are those commonly used in high-technology industries, development of super alloys and clean energy or elements that replace heavy metals in petroleum fracking (Hein et al., 2013). In 2013, the European Union (EU) pointed out 54 elements as strategic elements (European Commission, 2016), including Co, V, Cd, Te, Ba, Ni, REY and PGEs. These strategic elements are defined as metal or chemical elements used in the industry for their particular intrinsic characteristics and are needed by all industrialized countries (Adachi et al., 2010; Massari and Ruberti, 2013). This makes Fe-Mn crusts a potential resource for many of the metals used in emerging high-technology and green-technology applications (Hein and Petersen, 2013). However, only the purely hydrogenetic crusts contain sufficient rare metals to be of current economic interest (Hein et al., 2000).

Regulations for prospecting and exploration for cobalt-rich Fe-Mn crusts in areas beyond national jurisdictions (referred to as 'the Area') were approved at the ISBA's Eighteenth Session in 2012 (ISBA/18e/A/11). Several exploration contracts for cobalt-rich Fe-Mn crusts on Pacific and South Atlantic seamounts have been signed.

This paper presents a comprehensive study of Fe-Mn crust deposits on four seamounts (Tropic, The Paps, Drago and Echo) with summits ranging from 250 to 2400 m water depths within the Canary Island Seamount Province (CISP) in the northeastern tropical Atlantic. >100 seamounts compose the CISP from 23° to 33° N. The studied seamounts, which are the oldest of the CISP (ranging from 91 to 119 Ma), are located along the southern side of the CISP within the Spanish EEZ and Extended Continental Shelf, submitted by Spain on 14 December 2014 to the Commission on the Extension of the Continental Shelf. We herein present the results corresponding to a full suite of Fe-Mn crusts based on detailed mineralogy, petrography and chemical analyses, including major oxides, minor elements, REY and PGEs. Furthermore, we present multibeam bathymetry echosounder (MBES) mosaics of the seamounts where the crusts were collected between 1700 and 3000 m water depths. Crust growth rates and ages were estimated using the Co-Chronometer. Finally, we propose genetic models for the Fe-Mn crust deposits and correlate the latter to key paleoceanographic and tectonic events that occurred in the North Atlantic since the late Cretaceous.

2. Geological and present-day oceanographic setting

2.1. Geological setting

The studied area is located on the southern side of the Canary Islands. The CISP islands and seamount cluster form one of the most important volcanic provinces in the Atlantic Ocean (Fig. 1). The CISP consists of >100 seamounts that extend along 1000 km from the Lars-Essaouria seamount in the north (32.7°N, 13.2°W) to the Tropic seamount in the southwest of the archipelago (23.8° N, 20.7° W), following a general SW-NE orientation 100 km west off the African coast (Fig. 1B). The CISP formed by recurrent shallow mantle upwelling beneath the Atlantic Ocean basin, which produced recurrent anomalies and seamounts from the Early Cretaceous to the present day, making CISP the oldest active hotspot track in the Atlantic Ocean and the most long-lived preserved on Earth (van den Bogaard, 2013).

Volcanism in the Canary Islands Archipelago is of alkali type, which is characteristic of oceanic islands (Carracedo et al., 2002; Ancochea, 2004). The studied southwest Canary Islands seamounts are compositionally similar to the islands (Schmincke et al., 2000; IGME, 2015), also indicating intraplate alkalic volcanism.

2.2. Modern circulation in the CISP region

The CISP forms an important oceanographic regime in the tropical Atlantic, which includes both the oligotrophic waters of the eastern North Atlantic subtropical gyre and the productive, seasonal coastal upwelling zones of Morocco-Sahara (Henderiks, 2001). The mixed layer (upper 100 m of the water column) is characterized by the Canary Current (CC). The intermediate depth is ventilated by North Atlantic Central Water (NACW) and South Atlantic Central Water (SACW) above ~700 m and Antarctic Intermediate Water (AAIW) at ~1000 m. The North Atlantic Deep Water (NADW) fills the depth below 1500 m and the AABW occurs below ~4000 m (Fig. 1) (Machín et al., 2006; Pastor et al., 2015; Sarnthein et al., 1982; Hernández-Guerra et al., 2005; Knoll et al., 2002). In addition, the study area is beneath the northern end of the oxygen minimum zone (OMZ), which extends from 100 to 700 m water depths, from near the equator to 25° N. The core of the OMZ is located at 400–500 m, reaching very low oxygen values (<50 μmol/kg) (Brandt et al., 2010, 2012). The currents ventilating the OMZ are the NACW and SACW. These two currents have dissolved oxygen contents (DO) of around 200 μmol/kg in more proximal areas (Mémery et al., 2000; Bashmachnikov et al., 2015). Depletion in DO contents within the OMZ depend on interferences from less oxygenated water masses such as the Mediterran Outflow Water (170 μmol/kg) and AAIW (110 μmol/kg). DO is also depleted by the high biological productivity in proximity to the Canary Islands produced by upwelling and nutrient-rich currents (Brandt et al., 2010; Bashmachnikov et al., 2015).

3. Materials and methods

3.1. Sampling site description

Fe-Mn crusts were collected on board the R/V *Miguel Oliver* in 2011 during the DRAGO0511 cruise using a rectangular rock dredge (2 × 0.8 m) (Project for the Extension of Spain's Continental Shelf westward from the Canary Islands). Dredging sites were previously selected on the basis of the 3D models of bathymetry and backscatter data acquired with the Konsberg-Simrad EM302 echo sounder during the cruise. Submarine images and HRS (TOPAS PS 018) profiles were also obtained, which indicated the presence of hardground encrustations along the slopes and summits on the four seamounts: Echo, Tropic, Drago and The Paps. These high-resolution bathymetric data show two different morphologies. Tropic and Echo have typical guyot morphology showing flat summits. Sub-aerial exposure and erosion above sea level is supported for Echo and Tropic seamounts (conglomerates, shallow water calcarenites and guyot-like flat tops) (Schmincke et al., 2000; IGME, 2015). The Paps and Drago seamounts show ridge-like morphologies with multi-crest summits and were emplaced below sea level. Linear volcanic alignments along eruptive fissures and faults are commonly perpendicular to the least compressive stress and frequent in the Canary Islands (Delaney et al., 1986; Becerril et al., 2013, 2015). A detailed description of the morphology of the seamounts based on the multibeam bathymetry of the project can be found in Palomino et al. (2016).

The Tropic rises from 4300 to 970 m and has a surface area of 1530 km^2; its base morphology shows a four-arm star due to landslide scars

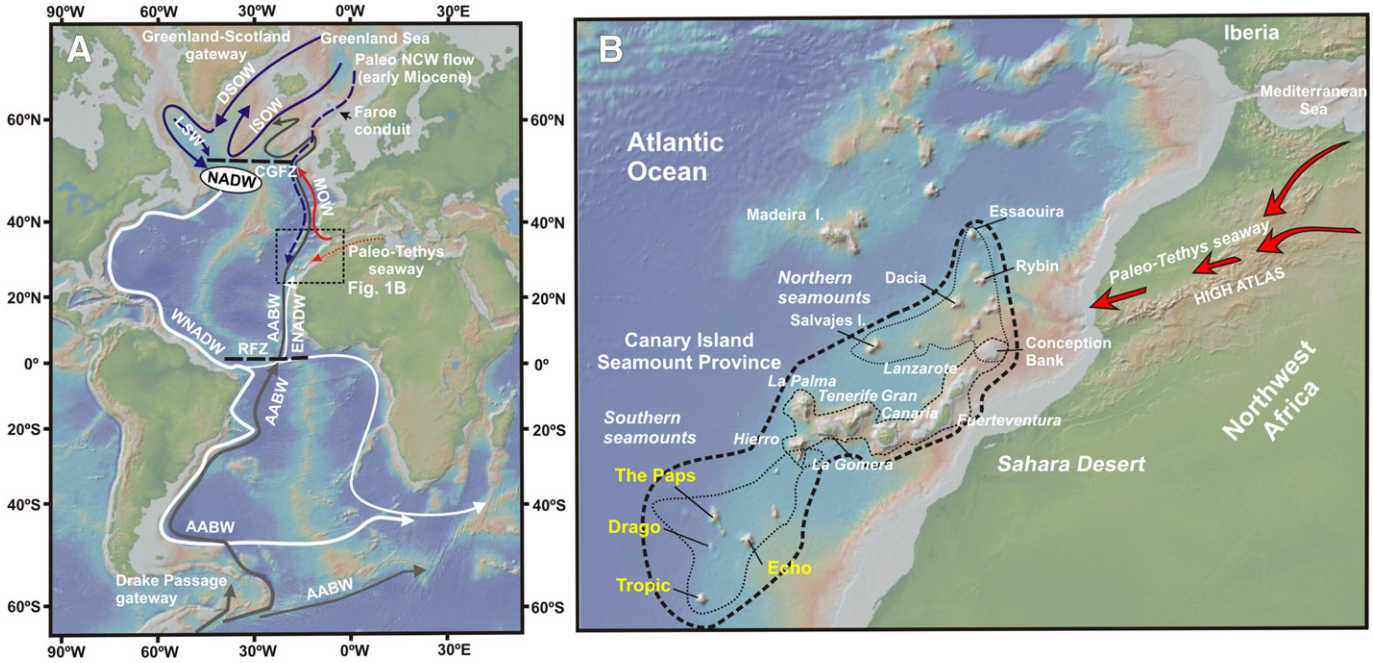

Fig. 1. Setting of the Canary Island Seamount Province (CISP). A) Pathways of principal currents along the Atlantic margins: NADW-North Atlantic Deep Water, ENADW-Eastern North Atlantic Deep Water; AABW-Antarctic Bottom Water, MOW-Mediterranean Outflow Water (Based on Abouchami et al., 1999 and Müller-Michaelis et al., 2013). B) Location of CISP formed by two seamount groups to the north and south of the Canary Islands. The CISP is the oldest hotspot track in the Atlantic Ocean (van den Bogaard, 2013), located close to the African continental margin within the area of influence of the Paleo-Tethys seaway and the Sahara Desert. Sampled seamounts are marked in yellow. See text for detailed explanation.

(Palomino et al., 2016). Samples DR15 and DR16 were dredged from 2287 to 2263 m along the southern arm and at 1719 m along the eastern arm respectively (Table 1 and Fig. 2A).

Echo seamount rises 3700 to 250 m and has a total surface area of 1400 km^2 and is also topped by a flat summit with several small volcanic cones-domes. Landslide scars can also be identified (Palomino et al., 2016). Fe-Mn crusts were dredged along the slope of spurs identified along the north (DR02), west (DR04) and south (DR03) flanks of the seamount between 1949 and 1593 m water depths. (Table 1 and Fig. 2B). Fe-Mn crusts from the summits of both flat-topped seamounts were not recovered, possibly because of sediment accumulation. Sedimentation on the summit inhibits the formation of Fe-Mn crusts. Volcanic rocks were sampled from the cones-domes projecting from the flat summit, which showed very thin Fe-Mn crusts (<5 mm).

The Paps seamount has an elongated N-S morphology with a narrow ridge extending in a NW-SE direction (Fig. 2C). This seamount rises from 4400 to 1500 m and has an area of 2150 km^2. Fe-Mn crusts were mainly recovered from the northern flank (DR07, DR09, DR10 and DR11) via dredging from 2340 to 1860 m (Table 1 and Fig. 2C). Only one dredge (DR14) was collected along the southern ridge of the Paps seamount from 2221 to 2157 m water depth.

Drago seamount rises from 4400 to 2200 m, showing an elliptic morphology with a NNW-SSE trend. This seamount covers an area of 315 km^2 (Fig. 2D). Fe-Mn crusts were recovered only from one sampling site (DR13) from the summit of this seamount at 2426–2290 m water depth due to limitations of cable length (Table 1 and Fig. 2D).

A total of 16 Fe-Mn crusts were selected as representative of a large quantity of fragments from eleven dredge stations (Table 1) on the four

Table 1
Dataset of the most relevant characteristics of the dredge stations selected for this study, growth rate and approximate maximum age calculated for CISP Fe-Mn crusts using the Cobalt Chronometer proposed by Manheim and Lane-Bostwick (1988).

DREDGE-sample	Seamount	Latitude	Longitude	Water depth (m)	Co (μg/g)	Thickness (mm)	G. R. (mm/Ma)	Calc. age (Ma)
DR 02-9	Echo	25° 29,62′N	19° 23,47′W	1890–1875	5157	50	1.66	30
DR 03-1		25° 15,10′N	19° 23,55′W	1949–1757	5375	30	1.15	26
DR 04-14		25° 19,51′N	19° 18,92′W	1832–1593	4245	35	2.27	15
DR 07-8	The Paps	25° 57,18′N	20° 21,73′W	1860	3560	80	1.33	60
DR 09-10		26° 00,80′N	20° 21,57′W	2340–2198	4239	20	1.50	13
DR 09-11		26° 00,80′N	20° 21,57′W	2340–2198	3767	60	2.00	30
DR 10-7		26° 07,09′N	20° 19,75′W	3010–2839	4502	60	1.96	31
DR 11-2		25° 57,68′N	20° 19,18′W	1957–1952	4230	30	0.80	38
DR 13-11	Drago	25° 13,60′N	20° 24,90′W	2426–2290	3359	35	1.89	19
DR 13-12		25° 13,60′N	20° 24,90′W	2426–2290	4887	110	1.83	60
DR 13-13		25° 13,60′N	20° 24,90′W	2426–2290	5090	85	1.85	46
DR 14-1	The Paps	25° 39,25′N	20° 07,45′W	2221–2157	6745	30	1.12	27
DR 15-14A	Tropic	23° 46,18′N	20° 43,17′W	2287–2263	3834	70	2.67	26
DR 15-15		23° 46,18′N	20° 43,17′W	2287–2263	4664	70	2.10	33
DR 16-5		23° 52,91′N	20° 37,07′W	1719	1834	40	1.20	33
DR 16-13		23° 52,91′N	20° 37,07′W	1719	7169	90	1.19	76

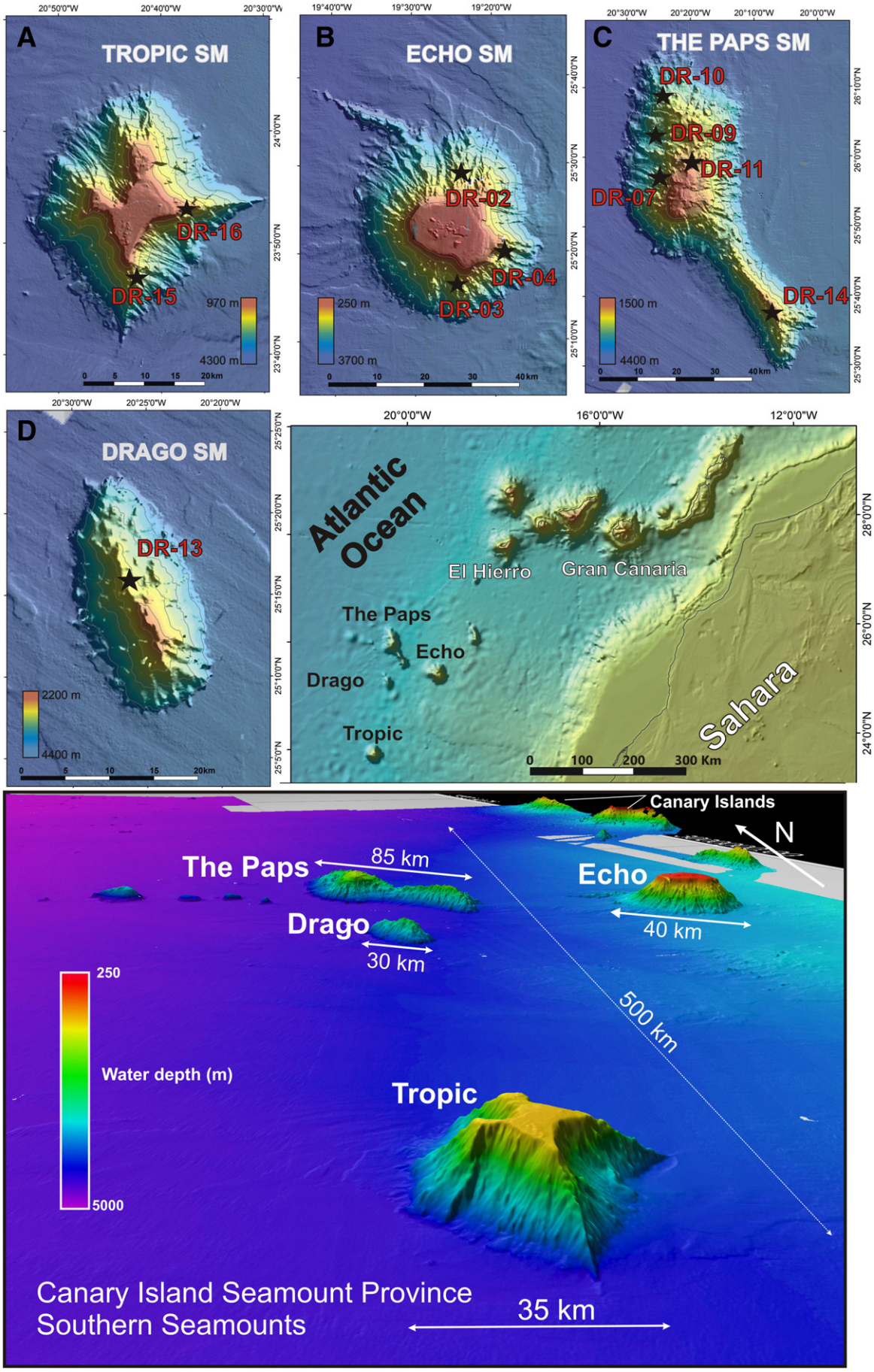
A
TROPIC SM
DR-16
DR-15
970 m
4300 m
B
ECHO SM
DR-02
DR-04
DR-03
250 m
3700 m
C
THE PAPS SM
DR-10
DR-09
DR-11
DR-07
DR-14
1500 m
4400 m
D
DRAGO SM
DR-13
2200 m
4400 m
Atlantic Ocean
El Hierro
Gran Canaria
The Paps
Echo
Drago
Tropic
Sahara
0 100 200 300 Km
Canary Islands
N
The Paps
85 km
Echo
40 km
Drago
30 km
500 km
250
Water depth (m)
5000
Tropic
Canary Island Seamount Province
Southern Seamounts
35 km

Fig. 3. A–B) Suite of Fe-Mn crusts collected from The Paps (DR07) and Drago (DR13) seamounts. C) Thick Fe-Mn crust on basaltic substrate. D and E) Phosphatized Fe-Mn crusts recovered from Tropic seamount. F) Cross section of Fe-Mn crust covering a carbonate substrate.

seamounts. The selected Fe-Mn crusts show thicknesses ranging from 20 to 110 mm, with colors that vary from dark brown to black and botryoidal surfaces (Fig. 3A–B).

3.2. Laboratory methods

Petrographic, mineralogical and geochemical methods were performed at the Central Laboratories of the Geological Survey of Spain (IGME), the Electron Microscopy National Center (UCM) and the Department of Crystallography and Mineralogy, Faculty of Geosciences (UCM). Mineralogical identifications were performed by X-ray powder diffraction (XRD). The equipment used included a PANalytical X'Pert PRO diffractometer, Cu-Kα radiation, carbon monochromator and automatic slit (PTRX-004). The analytical conditions for the XRD were: CuKα radiation at 40 kV and 30 mA, a curved graphite secondary monochromator, scans from 2 to 70 (2θ), step size of 0.0170 (2θ) and step time 0.5°/min.

Electron microscopy was used on polished thin sections using a Jeol JXA-8900 M Electron Probe WDS/EDS Micro Analyzer, operating at 15 EDS, equipped with four wavelength dispersion spectrometers in which these crystals were placed, as follows: channel 1: TAP; channel 2: LIF; channel 3: PETJ; channel 4: PETH. Two geochemical transects

Fig. 2. High resolution bathymetry of studied seamounts including dredge hauls (stars): A) Tropic, B) Echo, C) The Paps and D) Drago; bottom, three-dimensional multibeam bathymetric image (Simrad EM302), Fledermaus visualization of the seabed structure map in the study area. Viewing direction is from the south.

along the growth axis were performed with EPMA on samples DR 10-7 and DR 13-11 for 308 and 225 layer analysis respectively. Standards included pure metals, synthetic and natural minerals, all from international suppliers, and the accuracy and precision obtained were above ±5%.

The major and trace elements for bulk Fe-Mn crusts were determined using X-ray Fluorescence (XRF), using PANalytical's Magix equipment with a rhodium tube and Major software (PTE-RX-001 Ed. 3) and Irons protocol. The accuracy of the data was verified using international standard reference materials, and precision based on duplicate samples was found to better than ±5%. Analytical conditions were 50 kV voltage and 50 mA. The patterns obtained were compared with certified international standards (USGS, NBS, CANMET, BCS). Na and Au were measured using a VARIAN FS-220 atomic absorption spectrometer and loss on ignition (LOI) was determined by calcination at 950 °C.

REY and PGEs contents of bulk samples were obtained using ICP-MS (AGILENT 7500 CE). The standard reference materials SO-1 (CCMET), GSP-1 (USGS) and BCR-1 (USGS) were used to test the analytical procedure for REY determinations. The accuracy and precision are better than 10% for all REY. The study of PGEs was conducted using the preparation method described by Jackson et al. (1990) and Li and Feng (2006) and results were recalculated considering mass interferences described by Whiteley and Murray (2005). The results are expressed in percentages for major elements, μg/g (ppm), for minor and trace elements and in ng/g (ppb), for PGEs (Table 3).

Published studies of Fe-Mn oceanic deposits suggest that a relationship exists between growth rate and chemical composition, especially for Co contents (Reyss et al., 1982; Halbach et al., 1983; Manheim and Lane-Bostwick, 1988; Hein et al., 2000, 2013; Hein and Koschinsky, 2014). Crust growth rates and ages were calculated by the empirical Co-chronometer method established by Manheim and Lane-Bostwick (1988) which closely match isotopic determinations. In addition to the Manheim and Lane-Bostwick formula, other variants exist such as the proposal by Puteanus and Halbach (1988), which was used to minimize the dilution factor caused by phosphorite enrichment in older layers. For phosphatized sample DR16-5, the Fe, Mn, and Co were normalized to 0.5% P, therefore making the calculation more accurate (Hein et al., 2016); 0.5% P is the concentration in the non-phosphatized crust from the same dredge haul, DR16-13. One limitation of this Co-chronometer method is that the equation does not measure possible hiatuses during the accretion process. Therefore, the calculated rates represent maximum values and the derived ages minimum values (Hein et al., 1990).

Pearson correlation coefficients were used to calculate coefficient matrices for the chemical data. For $n = 15$, correlation coefficients between −5 and +5 have no correlation at the 95% confidence level.

4. Results

4.1. Structure, mineralogy and petrography

CISP Fe-Mn crusts are dark brownish to black and generally matte, although in some samples a metallic luster occurs (Fig. 3). Most of the specimens are characterized by botryoidal surfaces with variable-diameter botryoids, in which deep-water specimens have larger botryoids (up to 5 cm diameter) than shallow water specimens (few mm diameter). The thickness of the Fe-Mn oxide layer varies from a patina to 25 cm. Both altered volcanic rocks and compacted sediment act as substrates for the accumulation of oxides (Fig. 3D, F). Sedimentary substrate rocks frequently show Mn dendrite impregnations. Thin, lighter colored layers are the result of precipitation of carbonate layers, siliciclastic inputs and/or diagenetic phosphorites, carbonate fluorapatite (CFA) and phyllosilicates (Fig. 3E–F). Phosphatized Fe-Mn crusts with replacements and veins of CFA that crosscut oxide layers are common on Tropic seamount crusts (Fig. 3C).

XRD results of the Fe-Mn crusts are summarized in the Table 2. These oxyhydroxide minerals show strong overlaps and low crystallinity (Fig. 4). Goethite [α–$Fe^{3+}O$ (OH)] is the most important mineral group identified in all samples. Its presence can be observed in the central area of the diffractograms (30–60° 2θ) as a large peak representing the existence of some minerals of this group, in particular amorphous feroxyhyte [$Fe^{3+}O(OH)$], ferrihydrite [$Fe^{3+}{}_{10}O_{14}(OH)_2$] and goethite. Peaks corresponding to manganese oxides that overlap with large goethite peaks can be recognized in the same area. Mn oxides are vernadite (δ-MnO_2) and todorokite [$(Na,Ca,K,Ba,Sr)_{1-x}(Mn,Mg,Al)_6O_{12}\cdot 3\text{-}4H_2O$]; their characteristic peaks are found in the area of higher spacing (~9 Å todorokite) and in broadening of the peaks identified in the diffractograms. Vernadite and todorokite show some characteristic peaks: vernadite has a peak at ~2.39–~2.45 and 1.42 Å and may sometimes be confused with feroxyhyte, whereas todorokite shows a peak similar to clay minerals at 9.4 Å and the maximum intensity peak at 4.74 Å. Minor amounts of buserite ($Na_4Mn_{14}O_{27}\cdot 21H_2O$) and asbolane [$(Co,Ni)_{1-y}(Mn^{4+}O_2)_{2-x}(OH)_{2-2y+2x}\cdot n\ H_2O$], which are usually inter-grown, can also be recognized on XRD. Quartz, calcite and anorthite feldspar were recognized as detrital minerals. Well-defined palygorskite [$(Mg,Al)_2Si_4O_{10}(OH)\cdot 4H_2O$] and occasionally carbonate fluor-apatite [$Ca_5(PO_4)_3F$] peaks are authigenic minerals. CFA is identified as accessory by XRD in three Fe-Mn crusts from the Tropic, Drago and The Paps seamounts (Table 2). Sample DR16-05 is essentially formed by CFA and minor proportions of Fe-Mn oxyhydroxides representing a phosphatized Fe-Mn crust.

Crust micro-structures are generally laminae from 2 to 10 μm that compose larger botryoidal and columnar (Figs. 5A1, 2-B) structures, or more sub-parallel laminar patterns (Fig. 5A-1). The base of some crusts in contact with the substrate rock generally shows concretions that uniformly cover the rock. Occasionally, micronodules with spherical and botryoidal morphology can be found within a carbonate matrix. The Fe-Mn layers are not always homogenous and may show color variations, more specifically in zonation that differentiates massive-dense laminated areas from more porous parts. Discontinuities and accretion layers showing discordance with underlying Fe-Mn oxyhydroxide laminations can be found in the samples (Fig. 5A, B and E).

SEM images show Fe-Mn oxyhydroxides with Fe-Mn mineral grain sizes smaller than SEM resolution. The morphology consists of different micro-botryoidal aggregates of Fe-Mn oxyhydroxides (Fig. 6A–B). Porous textures under the SEM correspond to hollows where phyllosilicates crystalized with a filamentous structure (palygorskite) (Fig. 6D) and also to accumulations of carbonate coccolith shells, detached plaques of *Isochrysidales* or *Coccolithales* (Fig. 6D). SEM has not shown bacteria films, but micrometer size tubular structures have been recognized (<2 μm), covered by Fe-Mn oxides, that may result from the activity of microorganisms (Fig. 6C).

EPMA analyses on selected Fe-Mn crust polished thin sections are identified by numbers in Fig. 5. Two different micro-textural features can be differentiated in the samples: 1) massive sub-parallel layers (Fig. 5A-1) and 2) columnar-botryoidal (Fig. 5A-2) layers, in which detrital minerals and/or foraminifera are recognized. Some minerals are intercalated in the oxide layers: quartz shows sharp edges and is eolian; rhombohedral authigenic calcite-dolomite; hematite or magnetite crystals with Ti contents up to 10% (titanomagnetite; Fig. 5C); volcanic glass (Fig. 5F-15); and *Foraminifera*, are included within the laminations (Fig. 5E-12). *Foraminifera* show, in some samples, a high degree of substitution by Fe-Mn oxides.

4.2. Geochemistry

The bulk chemical composition of the Fe-Mn crusts is provided in Table 3. The phosphatized crust DR16-5 is discussed separately because the composition is significantly different from that of the other 15 samples. Crusts have high contents of Fe (13 to 28 wt%) and Mn (8 to 22 wt%), with Mn/Fe ratios ranging from 0.5 to 0.96. The crusts have more SiO_2 (9.7 wt%) than Al_2O_3 (3.74 wt%), K_2O (0.56 wt%) and MgO (2.33 wt%). The crusts have mean contents of 1.61 wt% TiO_2, 1.78 wt%

Table 2
XRD mineralogy of crystalline phases from CISP Fe-Mn crusts. Major >25%; Moderate 10–25%; Minor <10%. CFA = carbonate fluorapatite.

Sample	Type	Thickness (mm)	Major	Moderate	Minor
DR 02-9	Bulk	50	Goethite, δ-MnO_2	–	Quartz
DR 03-1	Bulk	30	Goethite, δ-MnO_2	–	Quartz, Calcite, Phyllosilicate
DR 04-14	Bulk	35	Goethite, δ-MnO_2	–	Quartz
DR 07-8	Bulk	80	Goethite	δ-MnO_2, Quartz	CFA, Calcite, Phyllosilicate
DR 09-10	Bulk	20	Goethite	δ-MnO_2, Quartz	Phyllosilicate
DR 09-11	Bulk	60	Goethite	δ-MnO_2, Quartz	Phyllosilicate, K-feldspar
DR 10-7	Bulk	60	Goethite, δ-MnO_2	Quartz	–
DR 11-2	Bulk	30	Goethite, Calcite	–	δ-MnO_2, Quartz
DR 13-11	Bulk	90	Goethite	δ-MnO_2, Quartz, CFA	Calcite, Phyllosilicate, K-feldspar
DR 13-12	Bulk	110	Goethite, δ-MnO_2	–	Quartz, Calcite, Phyllosilicate
DR 13-13	Bulk	85	Goethite, δ-MnO_2	–	Quartz, Phyllosilicate
DR 14-1	Bulk	30	Goethite, δ-MnO_2	–	Phyllosilicate, CFA
DR 15-14A	Bulk	70	Goethite, δ-MnO_2	–	Quartz, Calcite
DR 15-15	Bulk	70	Goethite, δ-MnO_2	–	Quartz, Calcite
DR 16-5	Bulk	40	CFA	Calcite	Goethite, δ-MnO_2
DR 16-13	Bulk	90	Goethite, δ-MnO_2	–	–

P_2O_5, and 6 wt% CaO, although two samples have higher bulk contents of CaO and P_2O_5 (respectively 8.19–12.2 wt% and 3.78–6.4 wt%) and another crust has 25.3 wt% CaO due to the presence of carbonate rock fragments in the crust (Table 3). Al, Si, K, Mg and Ca are depleted by an order of magnitude compared to average composition of Earth's crust (Taylor and McLennan, 1985; Wedepohl, 1991).

Co shows the highest average content among the minor elements (0.47 wt%), and ranges from 0.33 to 0.72 wt%. The content of other minor elements are variable: Ba (1000–5800 μg/g), Ni (1500–6000 μg/g), V (1000–3600 μg/g) and Pb (800–2300 μg/g). Other economically important elements but with a lower average content are Cu (260–1600 μg/g), Mo (100–650 μg/g) and W (30–140 μg/g). The average concentrations of elements that are traditionally considered to be of greatest economic potential (Co, Ni and Cu) are 0.5, 0.3 and 0.1 wt% respectively. Recent studies indicate that several other critical metals in Fe-Mn crusts may be of economic interest including Mo, Nb, Tl, V, W, Pt and REY (Hein and Koschinsky, 2014; Hein et al., 2015). The total average content of Nb, V, Mo, W and REY is 0.6 wt% ranging from 0.3 to 0.8 wt%. Compared to average continental crust abundances (Taylor and McLennan, 1985; Wedepohl, 1991), several elements (Co, Ni, Mo, V,

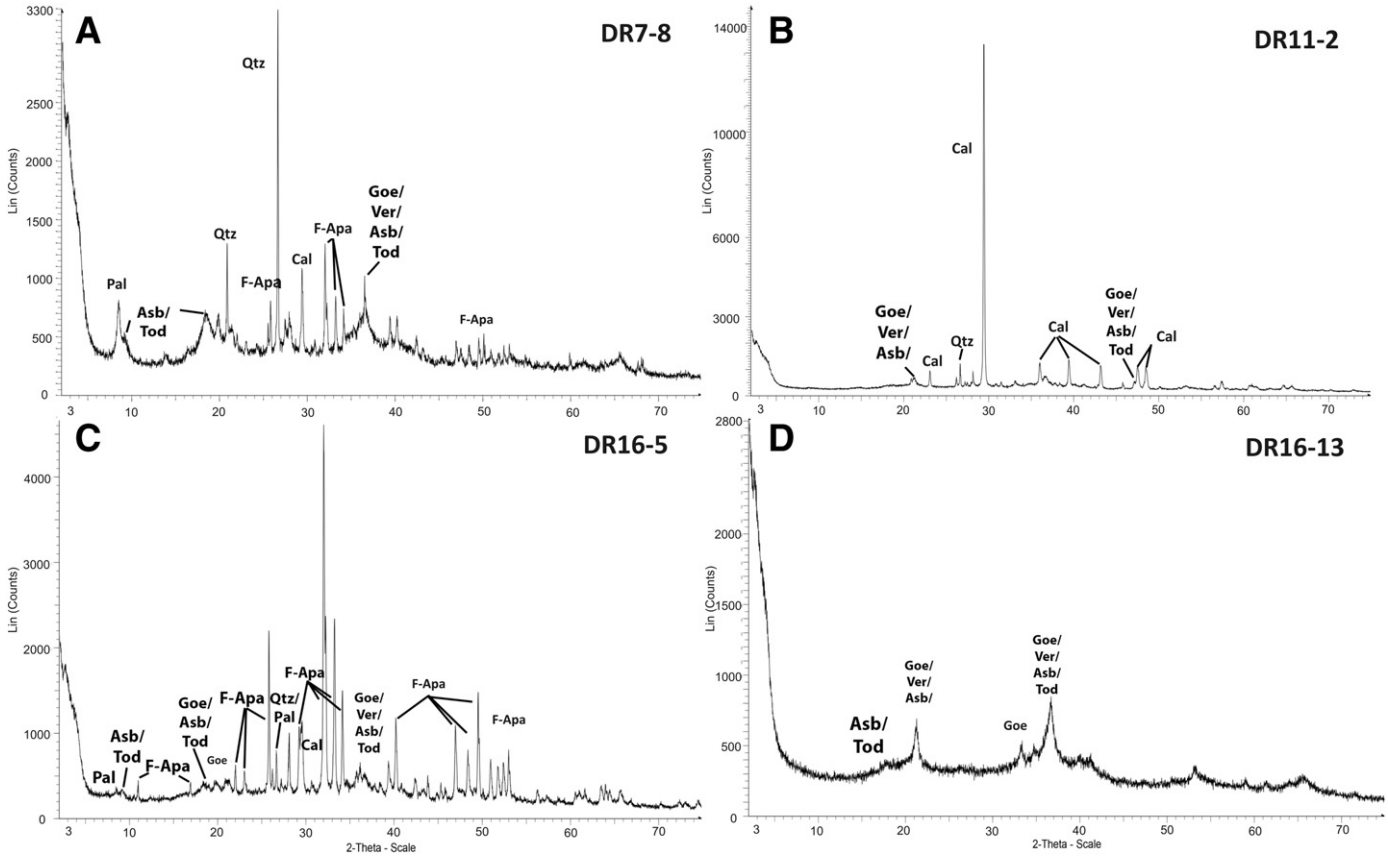

Fig. 4. XRD for studied Fe-Mn crusts. Fe oxy-hydroxides goethite group (Goe) appears essentially in the central part of the diffractogram. Mn minerals vernadite (Ver), asbolane-buserite (Asb) and todorokite (Tod) are superimposed on the same zone and also appear around the 8–10 Å zone. Crystalline minerals quartz (Qtz), calcite (Cal), fluorapatite (F-Apa) and authigenic palygorskite (Pal) are easily recognized.

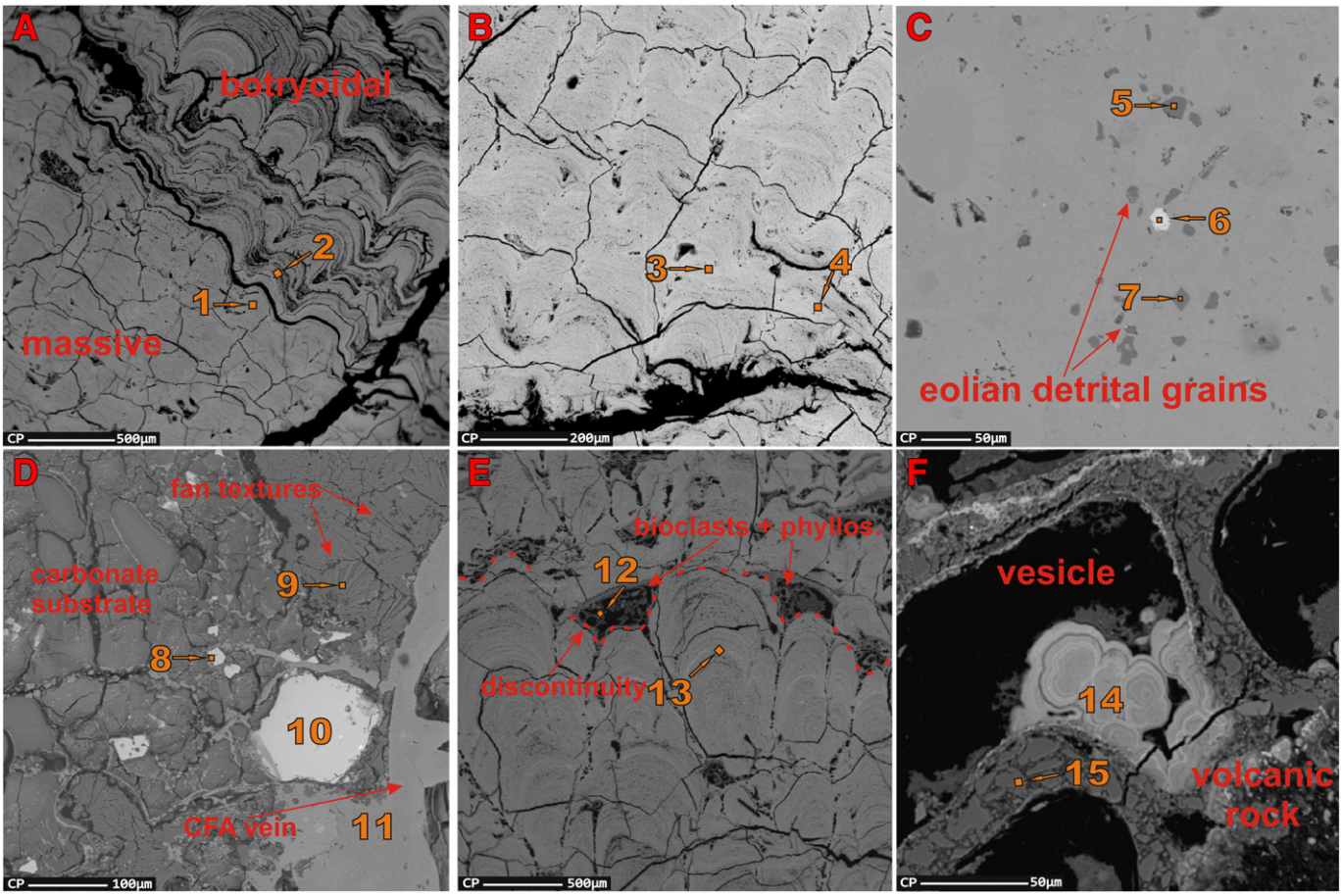

Fig. 5. Thin and polished-section EPMA photomicrographs of Fe-Mn crusts (backscatter mode) with location of microprobe analysis (see Supplementary Table 2). A) Massive-laminated texture rich in Mn minerals and botryoidal layered texture enriched in Fe oxyhydroxides. B) Layered oxide texture with different backscatter due to chemical variations in trace metal content. C) Eolian quartz, magnetite or maghemite and rhomboid dolomite. D) Magnetite or maghemite and typical fan morphology of palygorskite in a phosphatized crust. E) Bioclasts and phyllosilicates marking a discontinuity between accretion layers in the Fe-Mn crust. F) Mn rich oxyhydroxides in a volcanic vesicle formed in volcanic glass.

W and Cu) are enriched in the Fe-Mn crusts by up to two orders of magnitude (Fig. 7). Compared to other crusts studied here, crust sample DR16-13 is the most enriched in Fe + Mn (50 wt%), strategic metals Cu, Co, Ni, V, Mo and W (1.48 wt%), and REEs (0.35 wt%), and is Cretaceous, as discussed below.

REY contents are presented in Table 3. The distribution patterns of REY show moderate variations in total content, with LREEs being most abundant in all samples. Ce shows the highest average content (690–2200 µg/g) followed by La (170–420 µg/g) and Nd (140–380 µg/g). These elements have been normalized with respect to PAAS (Post-Archean Australian Shale) (Condie, 1993). Results plotted in Fig. 8A show LREEs and MREEs enrichment and a strong positive Ce anomaly typical of hydrogenetic crusts (Hein et al., 1988, 1997; Bau and Koschinsky, 2009). In addition, the samples show positive Gd anomalies. Compared to average continental crust abundances, La and Ce are enriched by one order of magnitude (Fig. 7).

PGEs bulk crust contents are in Table 3. The element with the highest content is Pt (103–321 ng/g), followed by Pd (1.17–171 ng/g). Rh and Ru show contents of 8.8–21 ng/g and 9–18.7 ng/g respectively. Pt shows a relative standard deviation of 35% and displays this variation in its concentration across all of the Fe-Mn crusts. Pd instead shows high standard deviation values that are indicative of great variability of concentrations. Au content was below the detection limit (0.1 µg/g) in all of the crusts analyzed except for sample DR10-7 with 2.3 µg/g. The PGEs mean content for all of the Fe-Mn crusts have been normalized to continental crust values (Wedepohl, 1995) and other Fe-Mn crusts from Indian and Pacific oceans. Canary Fe-Mn crusts are enriched in PGEs by more than two orders of magnitude compared to average continental crust, where Pt is enriched by three orders of magnitude, followed by Pd by two orders of magnitude.

Dredge DR16 (Tropic seamount) collected both phosphatized and non-phosphatized crusts. Pervasively phosphatized Fe-Mn crust (DR16-5) shows high CaO (33 wt%) and P_2O_5 (18 wt%) contents. Fe and Mn are 7 and 5 wt% respectively and with a low Mn/Fe ratio. This phosphatized crust is depleted in trace metals like Co, Ce, V and Mo in comparison with mean values and other non-phosphatized crusts from Tropic and other seamounts (Table 3). Additionally, the percentage of heavy (Eu through Lu) REY (HREY) to the total in the phosphatized crust (40 wt%) exceeds the percentage of HREY in non-phosphatized crusts (13 wt%). The characteristic patterns of this phosphatized Fe-Mn crust are HREY enriched, with a negative Ce anomaly and positive Gd and Y anomalies. All these patterns for REY are observed to a lesser degree in the other Fe-Mn crusts affected by less phosphatization (crusts DR7-8 and DR13-11). Phosphatized crusts show higher contents in PGEs than the average of the CISP crusts (Table 3).

The correlation matrix obtained for the compositional data of fifteen bulk crust samples (Supplementary Table 1) results in three distinct groups of elements having significant mutual association ($r > 0.5$ and < -0.5 at 95% confidence level). These are, a) Mn, Fe, Co, V, Zn, Mo, Pb, As and REEs, b) Si, Al, K, Mg and Na, and c) PGE. These element groups suggest that most of the minor elements and REEs in the CISP crusts are associated with a major Fe-Mn carrier phase, while the detrital element group (b) consists of separate minerals that dilute the oxide-group metals. On the other hand, PGEs do not show correlations with groups a and b elements and we speculate that they may form separate phases such as nanometer precious metal grains in Canary Fe-Mn crusts.

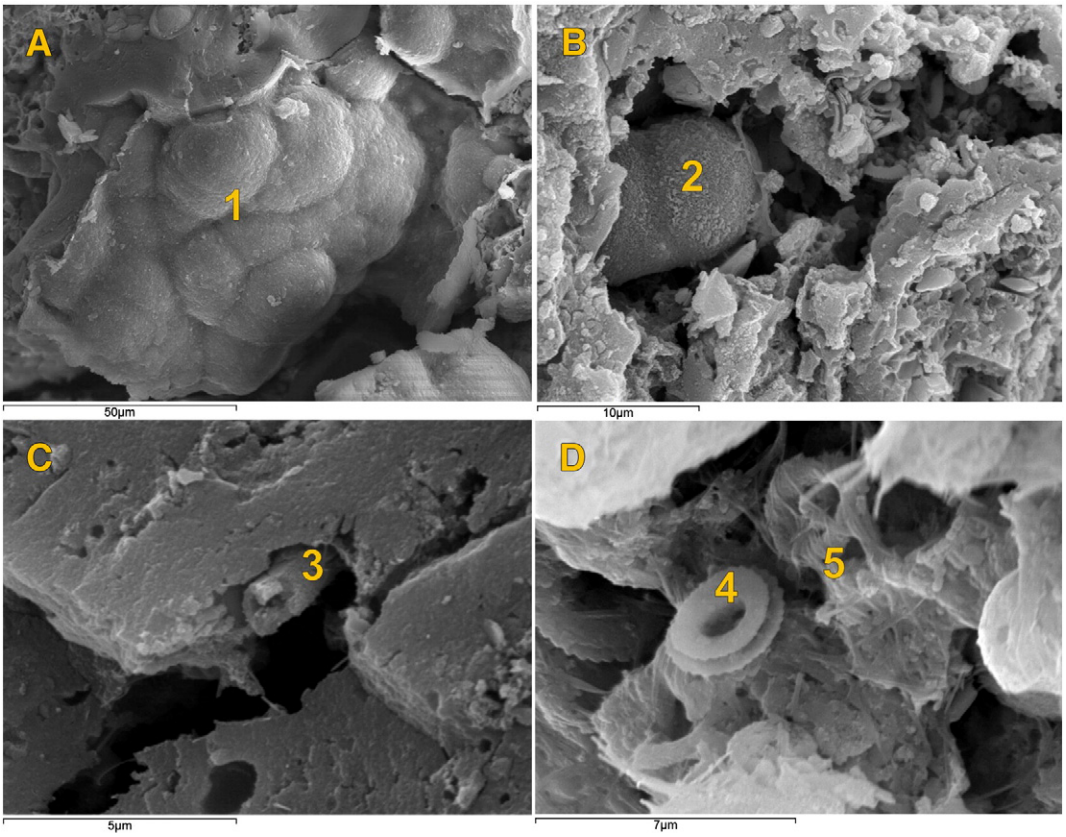

Fig. 6. SEM photomicrographs of Fe-Mn crusts. A-1) Micro-botryoidal texture of Fe-Mn minerals; B-2) globular Mn oxide in a fissure; C-3) tubular biological-like structure; D-4) coccoliths deposited on the Fe-Mn crust interlayer; D-5) palygorskite authigenic filaments formed in a Fe-Mn crust.

The massive layers studied using EPMA (Supplementary Table 2, Fig. 5A-1) show high Mn (21 wt%) and lower average Fe content (18 wt%) related to higher amounts of vernadite and other Mn oxides, while columnar-botryoidal layers have higher Fe (average 22 wt%) than Mn (19 wt%) (Fig. 5A-2), linked with the abundance of goethite-group minerals. The most reflective layers (backscatter in EPMA images) represent time intervals in which vernadite formed and enriched in Co (5 wt%) and high amounts of Ti (1 wt%) and Ni (0.4 wt%), while layers with low brightness have higher amounts of goethite (Fe content up to 25 wt%), V (0.3 wt%) and also subequal Ti (0.9 wt%). Precipitation of Fe-vernadite or todorokite also occurs in volcanic vesicles (Fig. 5F-14 Mn up to 26% and Fe 9%).

EPMA transects along the growth axis in crust DR10-7 show zones marked by differences in Fe and Mn content and also Si, Al, Co, Ni, Cu and P (Fig. 9; Supplementary Table 4). Several bands show higher contents of Fe (ranging from 25 to 34 wt%) that are also enriched in Si and Al (ranging from 1.3 to 2.6 wt% and from 1.3 to 2 wt% respectively) and slightly enriched in Cu and P (from 0.02 to 0.08 wt% and from 0.3 to 0.5 wt% respectively). These Fe-rich layers show a complex arrangement of oxide laminae, high porosity, and abundant microfossil tests. On the other hand, higher amounts of Co (ranging from 0.5 to 0.9 wt%) and Ni (from 0.2 to 0.4 wt%) have also been found in layers with higher contents of Mn (from 18 to 23 wt%). These Mn-rich layers show subparallel, dense, oxide laminae and are particularly abundant at the base and top of the crust.

4.3. Growth rate and ages

Co-chronometer calculated growth rates range from 0.8 mm/Ma to 2.7 mm/Ma (Table 1). The Echo seamount crusts show growth rates of 1.15–2.26 mm/Ma, whereas The Paps seamount crusts show growth rates for north face crusts range from 0.8 to 2 mm/Ma (5 crusts) compared to 1.13 mm/Ma (1 crust) for south side crusts. The Drago seamount crusts show growth rates of 1.8 mm/Ma, whereas the Tropic seamount crust growth rates range from 1.19 to 2.66 mm/Ma. The growth rate for DR16-5 falls within the ranges of the other samples; nevertheless, it should be used with caution even though it has been normalized for phosphatization (see Methods section). Based on the growth rates, the ages calculated for the initiation of Fe-Mn crust growth by bulk composition ranges from 13 to 76 Ma (Table 1), which are ages younger than the age of substrate volcanic rocks. Maximum calculated ages for crusts in the Tropic seamount are 76 Ma; The Paps, 60 Ma and Drago, 60 Ma. However, these ages are estimates and need to be verified using Os isotope dating otherwise the older ages can be off by many millions of years.

EPMA compositional transects along the growth axis for crusts DR10-7 (The Paps) and DR13-11 (Drago) show mean growth rates of 1.5 and 2 mm/Ma respectively, which are very similar to those calculated by bulk chemistry (1.96 and 1.89 mm/Ma respectively). Layer-by-layer ages for crusts DR10-7 and DR13-11 were 28 Ma, and 17 Ma, which are strongly coherent with the maximum ages obtained by bulk composition (30 Ma and 18.5 Ma respectively). This indicates that these crusts have grown at a remarkably constant rate. The average growth rate calculated in Fe-rich layers of these profiles was 1.7 mm/Ma, ranging between 1 and 3.8 mm/Ma, with local maxima of up to 4.5 mm/Ma. Mn-rich layers show a lower average growth rate of 1.2 mm/Ma, ranging from 0.5 to 2 mm/Ma (Fig. 9).

5. Discussion

The internal features as well as the mineralogical and geochemical data presented here allow us to propose a comparison with deep-seabed Co-rich Fe-Mn crusts from other ocean basins and tectonic settings around the World. We propose the influence of global and regional

Table 3
Chemical composition of selected CISP Fe-Mn crusts. <DL: below detection limit. – : no data.

	Echo seamount			The Paps seamount						Drago seamount		
Sample	DR2-9	DR3-1	DR04-14	DR7-8	DR9-10	DR9-11	DR10-7	DR11-2	DR14-1	DR13-11	DR13-12	DR13-13
Fe (wt%)	26.5	22.7	26	13.6	20.3	21.5	24.7	15.6	26.6	18.9	26.1	27.6
Mn	17.5	14.2	17.7	13	13.8	14.5	17.7	7.72	19	12.1	18.2	18.8
Mn/Fe	0.66	0.62	0.68	0.96	0.68	0.67	0.72	0.50	0.72	0.64	0.70	0.68
SiO_2	5.45	12.5	6.39	18.5	19.3	16.3	11.7	5.70	5.11	12.2	6.80	6.57
Al_2O_3	2.60	5.13	3.23	6.60	6.21	4.94	3.97	2.65	2.75	4.51	3.11	3.11
CaO	3.37	4.00	3.11	8.19	2.65	2.98	3.22	25.3	4.45	12.2	5.04	2.99
TiO_2	1.65	2.47	1.30	1.04	1.68	1.55	1.75	1.76	1.84	1.53	1.63	1.64
K_2O	0.43	0.90	0.50	0.75	0.88	0.69	0.50	0.27	0.41	0.95	0.45	0.51
MgO	2.21	2.96	2.26	4.48	2.73	2.51	2.04	1.79	2.25	2.00	1.96	1.98
P_2O_5	1.32	1.71	1.25	3.78	1.17	1.28	1.20	0.84	2.01	6.40	1.15	1.12
Na_2O	1.70	1.62	1.56	1.67	1.93	2.47	1.76	1.13	1.81	1.50	1.52	1.94
H_2O^-	12.9	10.7	11.8	7.56	10.5	11.2	12.4	6.06	11.4	8.71	10.3	11.7
LOI	26.9	23.9	26.3	22.9	23.6	24.7	25.7	31.1	25.7	22	26.2	25.9
Co (μg/g)	5157	5375	4245	3560	4239	3767	4502	4230	6745	3359	4887	5090
V	3072	2148	3143	1326	1862	2005	2465	1035	2446	1527	2568	2830
Zn	754	721	670	672	656	718	709	373	708	489	669	735
Ni	2443	2737	2252	6036	3238	2734	2756	1502	3558	1972	2420	2513
Cu	476	539	261	1573	969	637	771	479	798	555	651	926
Mo	456	354	511	214	282	355	379	103	440	283	454	504
W	100	91	129	38	44	28	90	29	115	50	114	138
Pb	2284	1707	2224	826	1307	1486	1736	828	1762	1157	1658	1861
As	478	433	479	255	379	389	416	325	470	310	439	458
Tl	72	87	137	95	95	61	71	50	116	56	81	112
Ba	4525	2893	4673	1701	2474	2649	3510	1031	2061	3906	4601	2964
Nb	98	138	97	116	119	100	125	154	122	100	101	123
La	380	343	397	172	222	276	330	189	422	330	390	412
Ce	1913	1663	1859	692	1329	1402	1694	1190	1773	1283	1834	2000
Pr	82.71	73.36	88.18	34.40	46.27	58.45	70.34	35.87	89.27	69.45	86.31	93.22
Nd	335	299	360	150	190	240	287	143	363	285	350	375
Sm	67.78	60.25	73.33	31.37	40.01	50.23	59.15	28.74	73.69	56.96	71.59	76.45
Eu	16.31	14.56	17.68	7.90	9.84	12.27	14.50	6.93	17.49	14.02	17.06	18.12
Gd	78.35	70.44	82.06	39.70	48.40	59.91	68.97	35.77	81.48	66.16	79.50	81.21
Tb	10.82	9.80	11.56	5.53	6.94	8.67	9.64	5.01	11.40	9.45	11.26	11.44
Dy	62.26	56.33	66.30	34.40	41.58	50.90	56.63	29.27	65.23	55.43	63.45	63.43
Y	199	220	239	225	171	209	201	120	264	285	226	219
Ho	11.95	11.12	12.81	7.33	8.30	10.34	11.06	5.82	12.75	11.06	12.04	11.89
Er	32.51	30.80	35.82	21.74	24.03	29.05	30.49	16.39	35.21	31.33	32.78	32.51
Tm	4.58	4.28	4.95	3.04	3.49	4.23	4.34	2.36	4.92	4.34	4.57	4.49
Yb	28.37	26.65	30.83	18.93	22.24	26.91	27.63	15.33	30.47	27.71	28.55	27.98
Lu	4.06	3.93	4.43	2.94	3.38	4.00	4.11	2.30	4.59	4.10	4.13	4.02
%REY	0.32	0.29	0.33	0.14	0.22	0.24	0.29	0.18	0.32	0.25	0.32	0.34
%HREY	13.9	15.5	15.40	25.3	15.7	17.0	14.9	13.1	20.1	14.9	13.8	16.2
Ce_{SN}/Ce_{SN}*	2.48	2.41	2.28	2.06	3.01	2.53	2.55	3.30	2.10	1.95	2.30	2.35
Ce**	0.37	0.36	0.34	0.28	0.45	0.38	0.38	0.49	0.30	0.26	0.34	0.35
Y_{SN}/Ho_{SN}	0.48	0.56	0.53	0.88	0.59	0.58	0.52	0.59	0.59	0.74	0.54	0.53
Ru (ng/g)	10.09	11.42	9.07	14.93	16.09	10.44	12.90	10.86	14.22	16.43	14.83	12.69
Rh	10.55	15.90	8.81	16.12	17.55	9.16	12.79	18.20	17.49	19.72	21.41	13.82
Pd	5.30	1.41	6.45	1.17	1.36	12.73	1.44	21.29	<DL	<DL	1.49	2.87
Os	1.00	1.21	0.65	0.93	1.36	0.77	1.07	1.25	1.57	1.87	1.04	0.59
Ir	3.19	3.80	2.74	3.99	4.27	2.65	3.59	4.27	4.33	4.94	5.45	3.78
Pt	291	160	108	222	213	112	146	159	159	173	321	208

* calculated according Bau et al. (2014).
** Ce anomaly calculated as $Ce^* = Log\ (Ce/(2/3La+1/3Nd))$.
[a] Hein et al. (2000).
[b] Baturin and Dubinchuk (2011).
[c] Muiños et al. (2013).

environmental/oceanographic conditions on the mineralization. Lastly, the integration of the full dataset allows us to establish a comprehensive genetic model for Fe-Mn crust formation and metal accumulation in the oceanographic and geotectonic context of the CISP.

5.1. Comparison with other marine Fe-Mn deposits

Fe-Mn crusts are found on seamounts, submarine banks and spreading ridges around the world including: the Pacific Ocean (Halbach et al., 1981; Baturin, 1988; Baturin et al., 2012; Bogdanov et al., 1995; Hein, 2004; Hein et al., 1997, 2000, 2010, 2013), the Indian Ocean (Banakar et al., 1997, 2007; Banakar and Hein, 2000; Rajani et al., 2005; Glasby et al., 2010) and the Atlantic Ocean (Dubinin and Rozanov, 2001; Canet et al., 2008; Baturin and Dubinchuk, 2011). Many seamounts along the Atlantic Spanish-Portuguese continental margins are known to have mineral deposits but are yet poorly studied (Koschinsky et al., 1995; González et al., 2012, 2014a, 2014b, 2016; Muiños et al., 2013; Marino et al., 2014).

Crust physical properties such as size, thickness, color, porosity and surficial textures are similar to Fe-Mn crusts reported for other deposits in world oceans (Hein et al., 1988, 2000; Banakar et al., 1997, 2007; Banakar and Hein, 2000; Rajani et al., 2005; Hein and Koschinsky, 2014). Laminar-massive and botryoidal-columnar morphologies (Fig. 3A and B) are similar to structures reported by Melnikov and Pletnev (2013) and Wang et al. (2015) for Pacific crusts. The formation of one structure over the other may depend on the presence of detrital

Tropic seamount				CISP crusts					Atlantic mean[a,b,c]	Pacific mean[a]	Indian mean[a]
DR15-14A	DR15-15	DR16-5	DR16-13	Mean	Min.	Max.	St. Dev.	St. Dev. (%)	n = 25 + 18 + 13	n = 2339	n = 14
26.5	27	6.98	28.3	23.45	13.6	28.3	4.56	19.46	18.84	19.27	23.6
16.9	18.8	4.92	21.7	16.11	7.72	21.7	3.53	21.92	14.68	21.37	15.6
0.64	0.70	0.70	0.77	0.69	0.50	0.96	0.10	13.91	0.78	1.11	0.66
8.14	7.50	8.00	3.65	9.72	3.65	19.3	5.07	52.13	10.42	12.81	7.78
3.04	2.99	2.52	1.29	3.74	1.29	6.60	1.46	39.06	3.87	2.91	1.34
5.59	3.58	33	3.49	6.01	2.65	25.2	5.89	98.02	2.53	4.28	0.75
1.45	1.59	0.55	1.24	1.61	1.04	2.47	0.32	19.89	1.29	1.63	1015
0.45	0.40	0.49	0.33	0.56	0.27	0.95	0.22	38.74	2.1	0.74	2.32
1.89	2.04	1.79	1.90	2.33	1.79	4.48	0.68	29.12	2.17	2.04	1.72
1.19	1.21	18.08	1.09	1.78	0.84	6.40	1.46	81.85	1.43	1.56	0.38
1.58	2.12	1.38	1.77	1.74	1.13	2.47	0.31	17.62	1.9	2.32	2.24
11.6	13.2	3.95	12.6	10.85	6.06	13.2	2.01	18.54	11.2*	15.38	12.8*
26.8	26.7	17.4	27.1	25.71	22	31.1	2.17	8.45	–	28.73	–
3834	4664	1698	7169	4722	3359	7169	1086	23.01	3919.5	4770.75	3126
2643	2796	432	3614	2365	1035	3614	716	30.29	813.37	584	624
625	694	356	899	673	373	899	118	17.55	570.67	655.58	533
1994	2405	2481	2924	2766	1502	6036	1038	37.52	2326.85	3777.33	2558
395	542	490	387	664	261	1573	321	48.33	798.78	892.42	1254
437	457	136	644	392	103	644	133	34.01	383.89	435.92	330
95	106	32	84	83	29	138	36.62	44.12	79.63	79.44	78
1595	1819	337	2106	1624	826	2284	445	27.39	1128.13	1502	1058
469	412	99	563	418	255	563	78	18.66	316.28	329.08	181
60	60	31	127	85	50	137	28	32.43	106.31	100.36	89.4
3480	4086	1015	5841	3360	1031	5841	1286	38.29	1407	1997	1668
89	88	27	85	110	85	154	20	18.05	52.67	36.17	74
374	402	364	402.3	336	172	422	83	24.79	265.26	292.25	286
1762	1942	449.77	2176	1634	692	2176	386	23.62	1446.34	1157.08	1481
82.97	91.21	61	89.92	72.79	34.40	91.21	20	27.74	64.32	60.77	68.8
341	373	260.28	362	297	143	375	81	27.13	245.62	251.67	248
71.08	76.01	49.77	74.82	60.76	28.74	76.45	16.31	26.84	56.45	51.95	60.2
17.20	18.20	12.70	17.50	14.64	6.93	18.20	3.77	25.78	11.96	15.79	10.8
80.81	84.76	63.72	77.57	69.01	35.77	84.76	16.07	23.28	62.15	52.92	62
11.43	12.09	8.75	10.69	9.72	5.53	12.09	2.25	23.15	9.54	8.83	9
66.33	68.87	56	59.72	56.01	29.27	68.87	12.08	21.57	49.53	52.96	49.4
246	229	557	173	215	120	285	40.10	18.65	167.31	179.75	163
12.79	12.90	12.49	11.07	10.88	5.82	12.90	2.13	19.62	9.7	9.53	9.8
35.09	35.01	37.69	29.63	30.16	16.39	35.82	5.51	18.26	28.5	28.4	26
4.90	4.87	5.18	4.06	4.23	2.36	4.95	0.74	17.50	3.78	4.03	3
30.45	30.17	33.63	25.05	26.49	15.33	30.83	4.46	16.84	24.08	26.24	22.7
4.37	4.23	5.28	3.48	3.87	2.30	4.59	0.61	15.73	3.8	3.54	3.46
0.31	0.34	0.20	0.35	0.28	0.18	0.35	0.06	22.63	0.24	0.22	0.25
16.2	14.8	40.1	11.7	15.5	11.7	25.3	3.22	20.93	15.13	17.40	14.35
2.30	2.33	0.68	2.63	2.44	1.95	3.30	0.35	14.32	2.41	1.89	2.3
0.34	0.35	−0.21	0.40	0.36	0.26	0.49	0.06	16.42	0.4	0.26	0.38
0.55	0.51	1.27	0.45	0.57	0.45	0.88	0.11	18.73	0.51	0.56	0.49
18.68	9.72	–	11.55	12.93	9.07	18.68	2.84	21.93	17.3	10.5	13
12.79	9.89	–	14.76	14.60	8.81	21.41	3.92	26.87	30.8	13	24
171	2.21	–	6.25	15.66	<DL	171	46.31	274.22	9.9	3.67	7
1.34	0.97	–	0.98	1.11	0.59	1.87	0.34	30.64	–	–	–
3.66	3.09	–	3.96	3.85	2.65	5.45	0.76	19.83	5.8	4.08	8
222	103	–	138	182	103	321	64	35.22	425	270.17	348

grains interrupting the lamination, promoting instead a columnar structure, or to the action of currents (Hein et al., 2000). The CISP crusts are characterized by Fe-oxyhydroxides (goethite type) predominating over Mn-oxides, while in samples from the Pacific Ocean the Mn oxide vernadite is predominant (Hein et al., 1997, 2000). This predominance of goethite-family minerals in the CISP crusts is similar to other locations from the Macaronesian area (Muiños et al., 2013). Quartz grains and other silicates present in the Canary crusts can be due to the input of eolian dust, as discussed below. Clay minerals, carbonates and CFA, abundant at the base of some crusts, are probably related to authigenic processes, as has been found for crusts from the Pacific or Indian oceans (Varentsov et al., 1991).

In contrast to the average geochemical values reported from Pacific, Indian and Atlantic Fe-Mn crusts (Hein, 2004; Baturin and Dubinchuk, 2011; Muiños et al., 2013), the CISP crusts show high Fe, V and Ba contents (Fig. 8C). Mn and Co are depleted compared to Fe-Mn crusts from the Pacific Ocean, but these elements are enriched in the CISP samples when compared to other Atlantic and Indian crusts. The average Mn/Fe ratio is 0.69 for the CISP crusts, lower than the mean ratio for Pacific crusts (1.11), and probably reflecting proximity to continental margins (Hein et al., 2000). The Cu and Ni contents are also lower than those reported for typical hydrogenetic Fe-Mn crusts, which reflects mineralogy. Pacific crusts show higher contents of vernadite and Fe-vernadite and amorphous Mn-feroxyhyte, which concentrate Ni and Cu in their

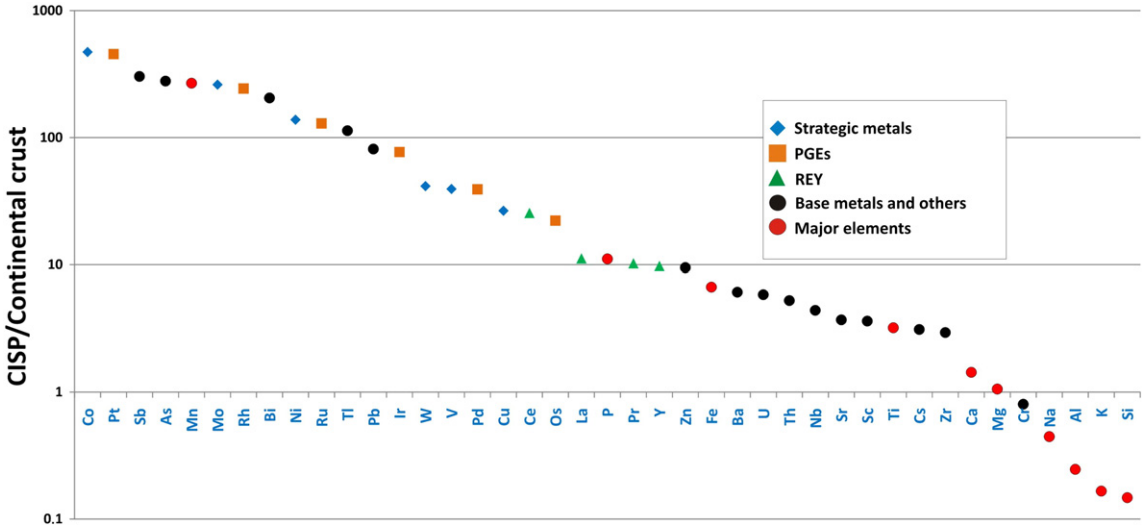

Fig. 7. Element enrichment diagram for composition of mean CISP crusts relative to composition of mean continental crust (Wedepohl, 1995); element ratios >1 are enriched in the CISP crusts and those below 1 are enriched in the continental crust. Elements arranged in order of decreasing element enrichment in the mean CISP crust dataset relative to the continental crust.

structures (Halbach et al., 1981; Bogdanov et al., 1995; Hein et al., 1997, 2000, 2010, 2013; Hein, 2004; Baturin, 1988; Baturin et al., 2012). Early diagenesis in crusts also favors an enrichment of these elements (Rajani et al., 2005). A comparison between REY contents in the CISP samples and other Fe-Mn crusts from other oceans (Bogdanov et al., 1995; Bau and Koschinsky, 2009; Muiños et al., 2013) is provided in Fig. 8D. Canary crusts exhibit enrichments in LREEs and MREEs when compared with Pacific samples, while HREEs are similar. REEs content in Canary crusts are slightly enriched in comparison with other Atlantic deposits (Muiños et al., 2013). The CISP samples show a strong positive

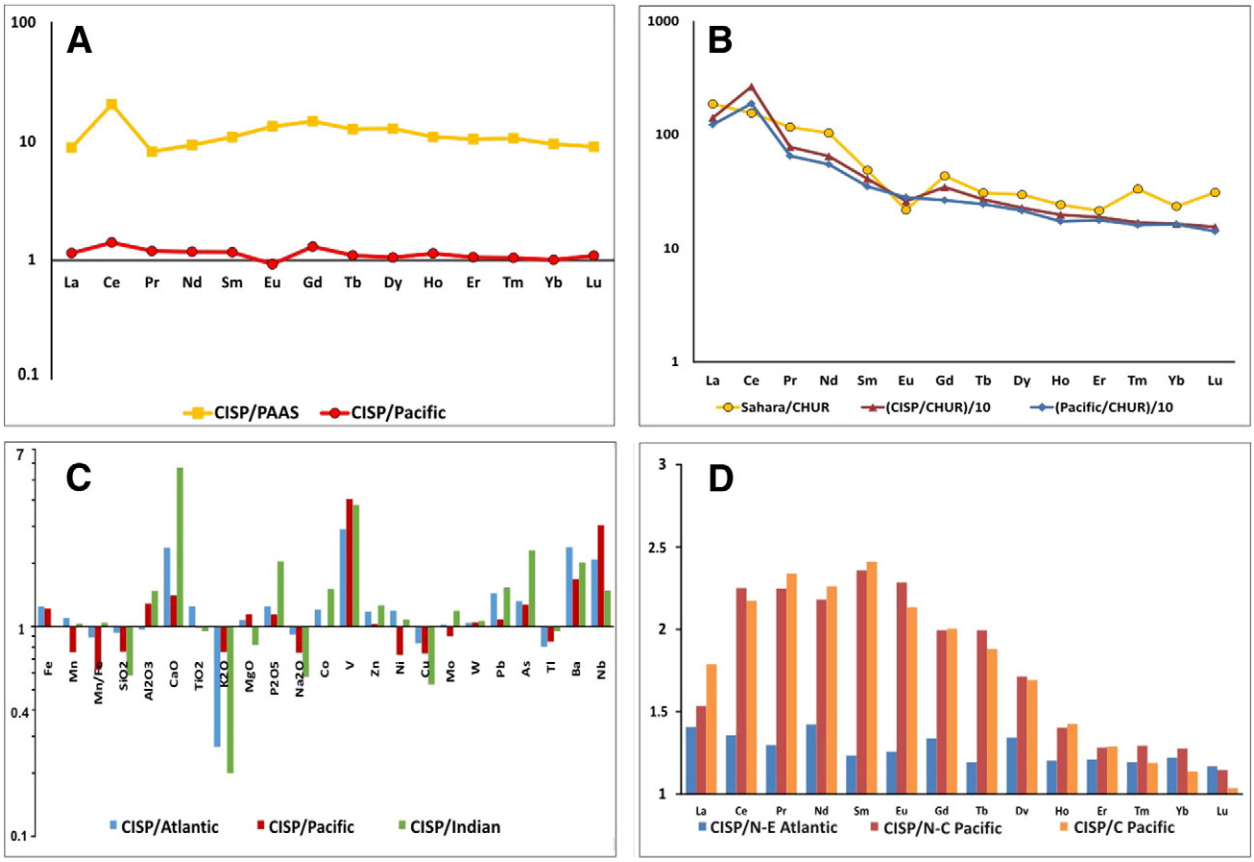

Fig. 8. A) PAAS and Pacific crust normalized REEs plots for Fe-Mn crusts from CISP; PAAS from Taylor and McLennan (1985). B) CHUR-normalized REEs plots for Saharan dust, CISP Fe-Mn crusts and Pacific average. CISP samples show similar patterns with Saharan dust except for Ce, which is strongly enriched in hydrogenetic crusts; CHUR data from Anders and Ebihara (1982). C) Element enrichment diagram for composition of mean CISP crusts relative to composition of mean Atlantic, Pacific and Indian Ocean crusts. Element ratios >1 are enriched in the CISP crusts and those below 1 are enriched in the other crust. D) REE enrichment factors with respect to Atlantic Ocean (Muiños et al., 2013), north-central Pacific Ocean (Bau and Koschinsky, 2009) and Central Pacific Ocean (Bogdanov et al., 1995). The crusts show large positive Ce anomalies characteristic of hydrogenetic precipitation.

correlation of REY with Fe, in accordance with the enrichment of Fe-minerals in the Canary crusts. PGEs contents reported from the Pacific and Indian oceans (Hein et al., 1988; Banakar et al., 2007) are higher than the values obtained in the CISP samples, although Pd is enriched in one crust that shows an atypically high content of 171 ppb. Halbach et al. (1989a) and Hein et al. (2000) stated that Pt ions react in a coupled reaction with Mn ions, becoming enriched in the δ-MnO_2 structure. They also propose that Pt depends on terrestrial inputs and its content in Fe-Mn crusts is directly correlated with the thickness of the crusts and inversely with water depth. This theory may explain why Canary crusts, which display a lower abundance of Mn oxides than Pacific samples, have also lower contents of PGEs.

Calculated Co-Chronometer bulk growth rates in CISP samples range between 1 and 2.7 mm/Ma, which agrees with the values obtained for Pacific or Indian crusts. The Fe-Mn crust DR16-13 from the Tropic seamount yields a maximum estimated age of 76 Ma (Late Cretaceous), therefore if this age is correct, it would be among the oldest crusts recovered from the ocean basins. Similar ages have been obtained for Fe-Mn crusts recovered on Mesozoic seamounts from the central Pacific Ocean (Ding et al., 2009; Nielsen et al., 2009; Hein and Koschinsky, 2014).

5.2. (Paleo) environmental conditions

5.2.1. Volcanic and hydrothermal activity

The older seamounts of CISP were formed during the Early Cretaceous 142 Ma ago (van den Bogaard, 2013) just after the opening of the Central North Atlantic mid-ocean ridge between the M25 and M21 magnetic anomalies (Late Jurassic, 156.6–149.9 Ma). Numerous magmatic-hydrothermal episodes have occurred since the late Mesozoic, which are related to the formation of islands and seamounts along the CISP (e.g., Schiffman and Staudigel, 1994; Lindblom and Gérard, 1998; Rodríguez-Losada et al., 2000; Donoghue et al., 2008; Hannington et al., 2016). We therefore suggest that successive Cenozoic hydrothermal-volcanic episodes may have exerted an influence over the growth of Fe-Mn crusts on the Cretaceous seamounts.

The volcanic eruptions in the CISP might therefore have contributed to increase dissolved metals in the seawater, sourced from magmatic and hydrothermal vents. This phenomenon has been recently evidenced by the high volume of gases (CO_2, CH_4, HS), Fe and other metals like Al (69 μg/L), Cu (20 μg/L), Zn (104 μg/L) and Mo (18 μg/L) released to the seawater during the 2011–2012 El Hierro submarine eruption (González, 2011; Santana-Casiano et al., 2013). An anomalous seawater plume, covering hundreds of square kilometers, was generated during the eruption, characterized by a low dissolved oxygen content (from 0 to 100 μmol kg^{-1} at 100 m water depth) and pH (down to 3) and high concentrations of dissolved Fe (>50 μmol kg^{-1}) and PO_4 (up to 0.6 μmol kg^{-1}) among other elements (Somoza et al., 2012; Santana-Casiano et al., 2013). Fe-oxide colloids and precipitates formed during the degasification, and low-temperature hydrothermal activity has been recently discovered covering the volcanic substrates of the eruption centers (González et al., 2014a, 2014b; Santana-Casiano et al., 2016; Hannington et al., 2016; Somoza and SUBVENT Scientific Party, 2014; Somoza et al., 2016 submitted). In comparing these, hundreds of similar eruptions throughout the last 142 Ma may have occurred, contributing with Fe and other metals to the seawater and increasing the formation of Fe-Mn crusts. Evidence of volcanic input is visible in the CISP Fe-Mn crust layers in the form of grains of volcanic rocks, probably sourced as lapilli-cinder from relatively close volcanic eruptions in the CISP. Evidence for hydrothermal input has not been identified from bulk crust geochemistry; a layer-by-layer EPMA composition of crusts would be necessary to identify geochemical-mineralogical signatures of these hydrothermal episodes, as observed in El Hierro submarine eruption.

5.2.2. The role of Sahara dust

The CISP is located within the zone influence of the Sahara, the largest desert and source of mineral dust on Earth (Helmers and Schrems, 1995; Eltayeb et al., 2001; Pohl et al., 2011; Scheuvens et al., 2013). Alumina-silicates, oxides and carbonates in the form of dust particles are transported by winds from the Sahara Desert into the Atlantic Ocean, influencing large areas. This phenomenon has been active since at least 8 Ma ago (Sincell, 1999; Sepulchre et al., 2006; Schuster et al., 2006), although some studies propose the existence of a previous proto-Sahara with a smaller extension since at least the late Oligocene dated at 23 Ma (Swezey, 1999; Kröepelin, 2006; Zhang et al., 2014). Sahara dust promoted detrital sedimentation on Fe-Mn crusts and acted as a source of chemical elements to the seawater that has also affected crust precipitation. Evidence of this input is visible in the CISP Fe-Mn crust layers as grains of quartz, feldspar and carbonate; these small detrital grains have been found both under the optical and electron microscopes (Fig. 5C). Other detrital minerals such as oxide or phosphate minerals sourced from Saharan dust are dissolved within the seawater column, contributing to the composition of these NE Atlantic crusts. Bulk geochemistry of Saharan dust and sands show that they are enriched in the same metals as the CISP crusts (Helmers and Schrems, 1995; Moreno et al., 2006; Castillo et al., 2008; Pohl et al., 2011; Scheuvens et al., 2013; Formenti et al., 2014). Geochemical studies of Sahara-sourced sands (Eltayeb et al., 2001; Mendez et al., 2010; Moreno et al., 2006; Muhs et al., 2010) show that minerals and aerosols, in addition to silica grains, have high Fe/Mn ratios. As a result, it would be reasonable to increase the availability of particulate and dissolved Fe and precipitation of Fe oxyhydroxides like goethite or feroxyhyte on seamount substrates. The occurrence of hematite or goethite in marine sediments sourced from Sahara dust has been confirmed in many studies (Grousset et al., 1998; Grousset and Biscaye, 2005; Kandler et al., 2011; Lázaro et al., 2008; Muhs et al., 2010). In addition, Sahara dust exhibits enrichments in P and Ti similar to that identified in the CISP Fe-Mn crusts (Supplementary Table 3). The enrichment in P, Ti, U, Th and correlation of the REEs pattern of Sahara dust with CHUR may be related to wind erosion of phosphate deposits localized in the West Sahara (Abed et al., 2009; Newman, 2011). Comparison of Sahara/CHUR ratio with the ones obtained in the samples studied in this work and the mean values for the Pacific are plotted in Fig. 8B. This comparison shows that CISP samples have the same negative Eu and positive Gd anomalies as Saharan dust, and suggests a genetic connection. These two anomalies are not always observed in Pacific samples.

The average Si/Al ratio on Fe-Mn crusts is 2.22, ranging from 1.64 to 2.92. Crusts from The Paps and Tropic seamounts show a higher average ratio (2.38 and 2.37 respectively) than in the Echo and Drago seamount crusts (1.92 and 1.73 respectively). In addition, northern Paps crusts (DR7-DR10) show a higher ratio (2.71) than the summit (1.9; DR11) and southern ridge crusts (1.64; DR14). The average Si/Al ratio on West Sahara dust was 5.7 (Supplementary Table 3; Scheuvens et al., 2013). This ratio is clearly higher than those of the CISP Fe-Mn crusts, therefore indicating the predominance of other processes in addition to the eolian input for the Si-Al component in crusts. These predominant processes may be related to the formation of authigenic phyllosilicate minerals, as observed in XRD and SEM images (Table 2 and Fig. 6D).

5.2.3. The role of the oxygen minimum zone (OMZ)

Dissolved Mn in seawater forms a reservoir in the OMZ. Water masses flowing northwards as the AABW or southwards as the ENADW (Fig. 1A) deliver oxygen-rich waters (Koschinsky et al., 1996). The development of OMZ around seamounts is an important factor for Fe-Mn crust formation (Halbach et al., 1981; Hein et al., 1988; Bogdanov et al., 1995). Thicker Fe-Mn crusts with higher strategic element contents grow on the tops and slopes of seamounts in or below

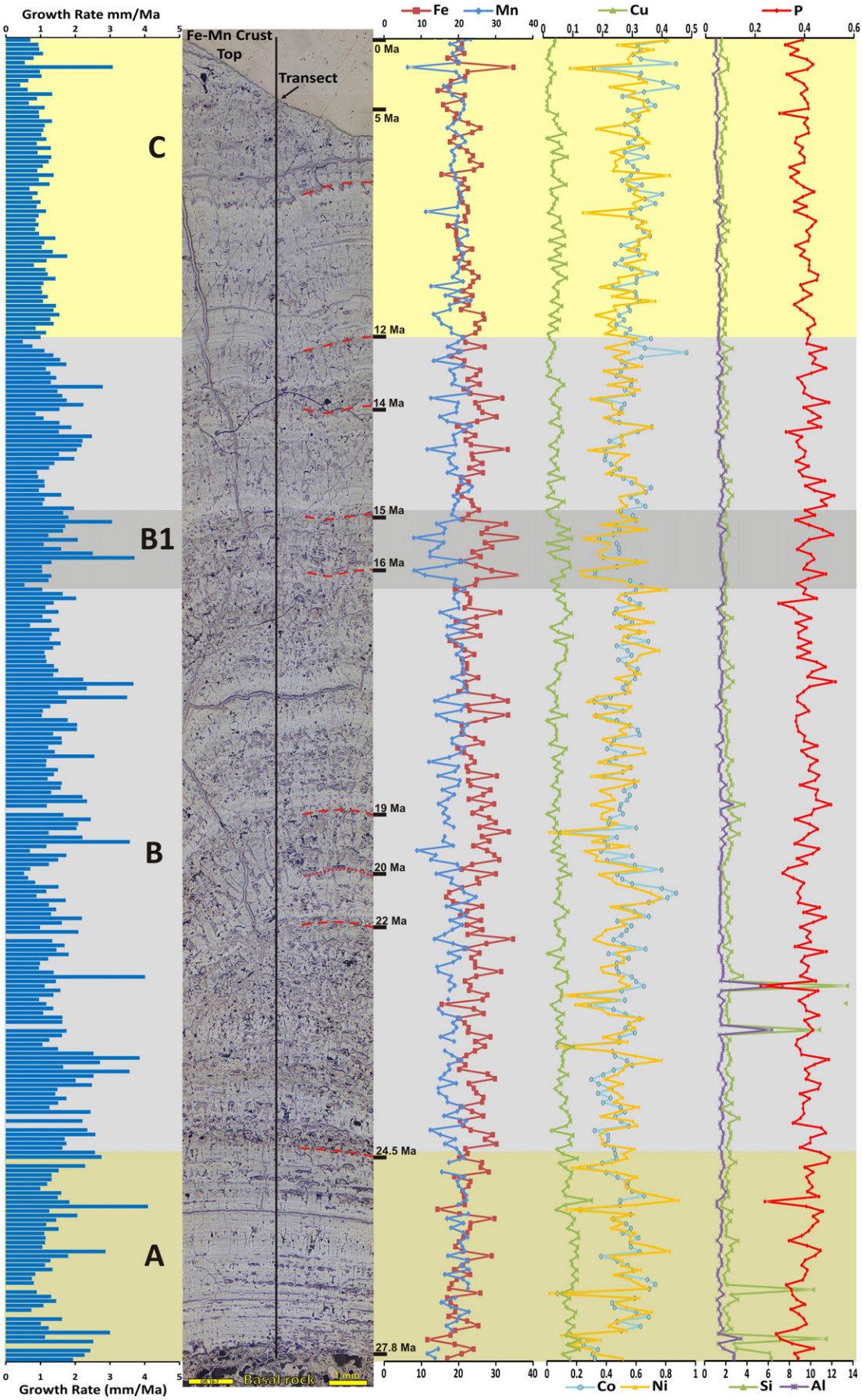
Growth Rate mm/Ma
Fe-Mn Crust Top
Transect
Fe
Mn
Cu
P
C
B1
B
A
0 Ma
5 Ma
12 Ma
14 Ma
15 Ma
16 Ma
19 Ma
20 Ma
22 Ma
24.5 Ma
27.8 Ma
Basal rock
Growth Rate (mm/Ma)
Co
Ni
Si
Al

the OMZ. The OMZ strongly depends on primary productivity that occurs in the photic zone, upper 200 m water depth. The OMZ ranges between 150 and 700–1000 m water depths, with low oxygen down to 1600 m water depths, where polar deep water masses have no influence (Bogdanov et al., 1990, 1995; Paulmier and Ruiz-Pino, 2009; Brandt et al., 2010, 2012).

A plot of the sample sites on a transect of seawater dissolved oxygen along the 23° N parallel (WOCE data) shows how all Fe-Mn crusts lie at deeper water depths than the northeastern tropical Atlantic OMZ core located at 400–500 m. This core of the OMZ with values as low as 50–100 μmol/kg extends from the equator to 23–25° N and is better developed in the eastern than the western side of the central North Atlantic, showing a clear eastward asymmetry. So, Echo seamount with its summit located at a mean depth of 350 m is bathed by the core of OMZ. The Paps and Tropic seamounts with summits at 1600 and 1000 m are bathed by moderate low oxygen values (150–200 μmol/kg). Drago seamount, with a summit at 2200 m is bathed by water masses with oxygen values of 200–225 μmol/kg. All Fe-Mn crust samples are located on lower increasing dissolved oxygen portion of the OMZ bathed by water masses with oxygen values ranging between 210 and 230 μmol/kg.

In general, a more extensive OMZ forces may promote slower growth rates of Fe-Mn crusts allowing more adsorption/enrichment of metals in the Mn-Fe oxyhydroxide structures, although this slowing of growth rates likely depends on the degree of depletion of dissolved oxygen (Conrad et al., 2017; Usui et al., 2017). Furthermore, the concentrations of many dissolved elements (e.g., Mn, Co, Ce, Cu, Pb and P) increase in the OMZ (Saager et al., 1997; Hein et al., 2000; Milne et al., 2010; Pohl et al., 2011). Conversely, Fe exhibits an opposite behavior that is explained by the presence at the same depth range of remineralization of biogenic material (Hatta et al., 2015). In the area studied, dissolved Co, Cu and Pb are enriched in the OMZ but decrease strongly below it (Aparicio-González et al., 2012). The fact that the Fe-Mn crusts are enriched in all of these elements suggests that former Cenozoic growth conditions were controlled by a stronger OMZ. Abundant coccoliths in the crusts (Fig. 6B, D) indicate significant upwelling and productivity above the seamounts, which contributed to the formation of a substantial OMZ during crust formation. Currently, the increase in total coccolith accumulation rates from a low of 1–2 g cm^{-2} ka^{-1} in the Canary Basin to 6–12 g cm^{-2} ka^{-1} closer to the Moroccan shelf was determined from Holocene sediments (Henderiks, 2001).

Past fluctuations in the extent of the OMZ in the east-central Atlantic controlling this enrichment in metals of the Fe-Mn crusts is related to three paleo-environmental factors and changes in global paleo-ocean circulation. First, the intensity of volcanic eruptions and hydrothermal activity on seamounts since the Cretaceous; second, the Sahara dust sourced from the African margin and its variation since Mio-Pliocene times; and third, the formation of and changes in the pathways and intensity of the global Thermohaline Circulation (THC) related to the influence of the northern and southern sources of oxygen-rich deep waters and the high salinity water mass of the Tethys/Mediterranean during Cenozoic times.

5.3. Relationship between growth process, geochemistry and Cenozoic ocean/continent evolvement

The specific analysis performed on sample DR 10-7 allows us to constrain certain geochemical variations through the Fe-Mn crust based on the layer-by-layer calculation of growth rates and geochemical parameters. Crust DR 10-7 shows a maximum age of 28 Ma (Fig. 9). This age coincides with the age from bulk samples from a large number of crusts across all seamounts ranging between 37.5 and 25.9 Ma (late Eocene-Oligocene).

5.3.1. Late Oligocene-early Miocene fertilization events due to increasing oceanic upwelling

The Eocene/Oligocene (E/O) marked the onset of a new circulation pattern characterized by the production of cold water masses in southern high latitudes that flow toward the deep Atlantic basins. (e.g. Maldonado et al., 2014). As ocean circulation intensified, the phosphorus-rich deep water was distributed to intermediate water depths by upwelling at the seamounts and may have been stored in the OMZ (Hein et al., 1993; Koschinsky et al., 1997).

We suggest that the layered interval in the middle of the EPMA profile between the 24.5 and 16 Ma correlates with the episodes of global phosphogenesis proposed by Hein et al. (1993): i.e. Two major and, possibly three minor episodes of phosphogenesis occurred from the late Oligocene to early Miocene (25–22 Ma) and the late-early Miocene (18–17 Ma). At a regional scale, in the NE Atlantic (Galicia Bank) three phosphatization generations forming hardgrounds were dated using $^{87}Sr/^{86}Sr$ and microfossils as late Oligocene (~25.7–24 Ma), early Miocene (23.8–22.6 Ma) and late-early Miocene (18.6–16.8 Ma) (González et al., 2016).

As a result, the crusts show several stratigraphic intervals displaying chaotic microstructures, and botryoidal, and porous structures with significant increases in Fe and P (average 23 and 0.43 wt% respectively) relative to other crust intervals. These layers show peaks of maximum growth rates of up to 4.5 mm/Ma and an abundance of bioclasts. This microfossil abundance indicates intensive primary productivity, probably related to the intermediate water ventilation of OMZ by upwelling of nutrient-rich currents (nitrate, phosphate, iron, etc.). These Fe-rich intervals are dated layer-by-layer at 24.5 Ma, 22–20 Ma, 19–16 Ma (Fig. 9). These data indicate that the Fe-rich intervals might be correlated with fertilization events characterized by high growth rates, probably caused by a decrease in the extent of the OMZ by the intrusion of deep currents (Fig. 9). In contrast, layered intervals that are particularly thick at the base and top of crust and defined by parallel lamination and well-defined columnar structures, display significant enrichment in Mn (up to 22 wt%), Co and Ni, a Mn/Fe ratio close to 1 (Fig. 9), and very slow growth rates (to 0.5 mm/Ma). We interpret these layered intervals as times of increases in the extent of the OMZ, which if low enough in depleted oxygen forced slower growth rates of the Fe-Mn crust and promoted more adsorption/enrichment of metals in the Mn-Fe oxyhydroxide structures (Hein et al., 2000).

Regarding the influence of the African continent, the occurrence of significant Si peaks in the interval between 27.8 and 22 Ma points to periods of detrital input sourced from the continent, since the Canary Islands were not yet formed at that time. These data support the existence of a previous proto-Sahara of smaller extension since at least the late Oligocene, at 23 Ma (Swezey, 1999; Kröepelin, 2006; Zhang et al., 2014).

5.3.2. Abrupt increase in Fe: Onset of the influence of Northern Component Waters on Canary seamounts

We suggest that the abrupt increase in Fe (up to 34 wt%) and decrease in Mn (down to 10 wt%) identified at the interval between 16 and 15 Ma may be related to the introduction of vigorous deep-water flow from the Arctic (Northern Component Waters, NCW) into the Atlantic basin. The Faroe conduit developed in the early Miocene was suggested to be the first true deep-water connection between the Nordic Seas and the Atlantic (Stoker et al., 2005). An abrupt inflow of NCW throughout the Faroe conduit would have allowed the NCW sourced in the Greenland Sea to flow directly along the eastern Atlantic Ocean

Fig. 9. EPMA transect across DR 10-7 Fe-Mn crust. Photomicrograph mosaic allows recognizing three stratigraphic intervals (horizontal color bands) with different structural styles. Differences in structure also are reflected in chemical composition and growth rate. For further explanation see text.

(Fig. 1A). The assumption of the onset of the introduction of Arctic deep waters during the late stages of the early Miocene (ca. 17–16 Ma) is supported by regional evidence of the breaching of the Greenland-Scotland Ridge, which is documented in several erosional unconformities in the NE Atlantic (e.g. Müller-Michaelis et al., 2013). In the Galicia Bank (NE Atlantic), the growth of hydrogenetic Fe-Mn crusts and nodules during the middle and late Miocene (17–16 Ma) followed the three previous events of phosphatization (González et al., 2016). This event in the North Atlantic Ocean is simultaneous to a deep-rooted mantle process responsible for the onset of the hotspot plume of the Canary Islands that formed the Fuerteventura (ca. 18 Ma), Lanzarote (ca. 15 Ma) and Gran Canaria Islands (ca. 15 Ma) (van den Bogaard, 2013) (Fig. 1B).

5.3.3. Slow growth rates: increase in OMZ extent in the NE Atlantic and stable thermohaline circulation

Another abrupt change identified along the EPMA profile occurred at about 12 Ma. This change is characterized by an abrupt decrease of the growth rates of the Fe-Mn crust (mean 1.1 mm/Ma) (Fig. 9) and an increase of Co content (up to 0.94 wt%), coupled with a slight enrichment in Ni and Cu (Fig. 9). After the opening of the Faroe conduit, the progressive opening of the Greenland-Scotland gateway as the Denmark Strait and Iceland-Faroe Ridge from the middle to late Miocene allowed the flow of the other branches of the NCW as DSO, ISOW and LSW (Fig. 1A) resulted in the formation and expansion of the NADW throughout the western North Atlantic Ocean. Pb and Nd isotopes from the Tropic Fe-Mn crusts show that the eastern Atlantic circulation along the African margin appears to be dominated by binary mixing from southern and northern sources throughout the last 13 Ma (Abouchami et al., 1999). Therefore, since the last 13 Ma, the NE Atlantic deep basins began to be ventilated by waters sourced from the Western North Atlantic Deep Waters (WNADW) flowing west-to-east through equatorial transform fault zones along the northwest African margin, forming the Eastern Atlantic Deep Waters (ENADW) (Abouchami et al., 1999) (Fig. 1A). The confluence between the Atlantic deep waters (ENADW) and the northern branch of the Antarctic Bottom Waters (AABW) are responsible for the stabilization of the present thermohaline circulation and, thus, led to an increase of the extent of the OMZ in the eastern tropical Atlantic margins since 12 Ma (Fig. 1A). As a result, we suggest that the progressive increase in thickness of OMZ may have initiated slower growth rates of the Fe-Mn crust identified in our EPMA profile, and promoted more adsorption/enrichment of metals (Mn up to 22 wt%) (Hein et al., 2000).

5.4. Genetic model

Numerous authors classified the oceanic Fe-Mn deposits using the ternary diagram Mn–Fe − (Cu + Ni + Co) × 10. According to this classification, Fe-Mn oxides can be diagenetic, with ratios of Mn/Fe > 2.5, rich in Cu and Ni, and poor in Co; hydrogenetic, in which Mn/Fe < 1 and with relatively high concentrations of Cu + Ni + Co with respect to the other genetic types; and hydrothermal, where Mn/Fe is either very high or very low, with the Fe-Mn deposits normally having low Cu + Ni + Co (Bonatti et al., 1972; Lyle, 1981; Dymond et al., 1984). The Fe-Mn crusts from the Canary seamounts plot in the hydrogenetic field on this ternary diagram (Fig. 10A) in an area superimposed by other samples from the Atlantic Ocean (Muiños et al., 2013) and more enriched in Fe than the crusts from the Pacific Ocean (Hein and Morgan, 1999).

The positive Ce anomalies can be explained by the input of a hydrogenetic Fe-Mn component. This component can be identified using the REY plots of Bau et al. (2014), where the Co-rich Fe-Mn crusts plot in the hydrogenetic (seawater-sourced) field (Fig. 10B and C). The Ce/La ratio is 1.2, similar to the ratios for seawater, indicating that REY and phosphate hosts were derived from seawater, probably within or near an oxygen minimum zone. This source is also consistent with positive Ce and positive Gd anomalies, (Fig. 8A, B) as occurs in other similar deposits from the Atlantic and Pacific oceans (Hein et al., 2000, 2013; Muiños et al., 2013). Some samples plot between the hydrogenetic and hydrothermal fields (Fig. 10C), corresponding to crusts with some degree of phosphatization.

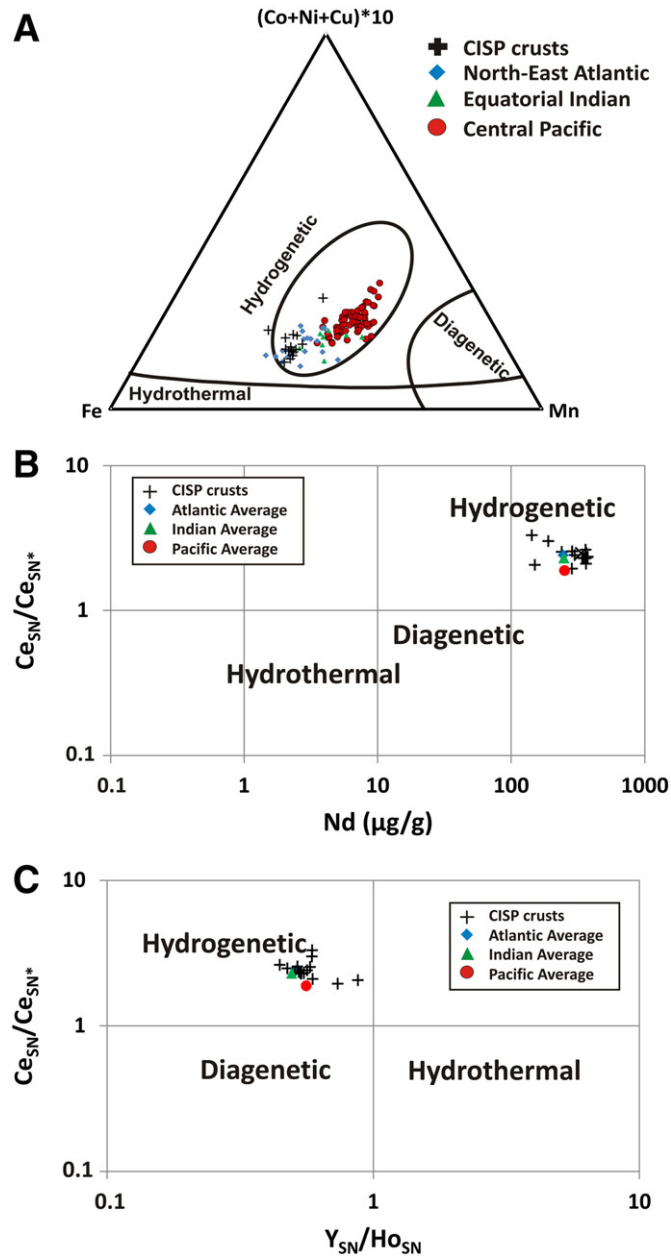

Fig. 10. A) Ternary plots for CISP crusts and other Fe-Mn crusts from the Atlantic (Muiños et al., 2013), Indian (Banakar et al., 2007) and Pacific Oceans (Hein and Morgan, 1999); ternary diagram modified from Bonatti et al. (1972) and the CISP crusts plot in the hydrogenetic field. B and C) Plot of Fe-Mn crusts on graphs of CeSN/CeSN vs Nd concentration and CeSN/CeSN vs YSN/HoSN ratios (after Bau et al., 2014) in comparison with Atlantic, Indian and Pacific deposits. The crusts plot in the hydrogenetic field on these diagrams.

The CISP samples are composed chiefly of Fe oxyhydroxides and secondarily of vernadite (Fig. 4), therefore confirming that the hydrogenetic processes were predominant in the genesis of these crusts. Small amounts of todorokite intergrown with asbolane and buserite have been detected in the CISP crusts, indicating a possible local diagenetic/hydrothermal process (e.g., Koschinsky and Hein, 2003; Canet et al., 2008; Baturin and Dubinchuk, 2011; Baturin et al., 2012; Hein et al., 2013; Wegorzewski et al., 2015), although todorokite can also occur in crusts formed within strong OMZs (Conrad et al., 2017). Minor quartz, feldspar, calcite and other detrital minerals (Fig. 5C-D) in the crusts are delivered by Sahara winds, while the formation of some clays such as palygorskite (Fig. 5D) depend on the

weathering of local outcrops and fragments of volcanic rock, which were also recognized by Varentsov et al. (1991). Some titanomagnetites of volcanic origin have also been detected as well as dolomite crystals with typical rhomboidal morphology (Fig. 5C–D). CFA is relatively abundant in some crusts (DR7-8; DR13-11; DR14-1 and DR16-5), indicating the presence of diagenetic processes. In the same way, authigenic phyllosilicates are present in crusts DR7-8; DR9-10 and DR13-11, therefore reflecting the importance of diagenetic processes.

5.5. Strategic element distribution in Fe-Mn crusts

The CISP Fe-Mn crusts are enriched in Fe and depleted in Mn relative to Pacific crusts. This is the main reason why Pacific crusts with higher vernadite, have more Co and Ni, while Atlantic crusts, including the CISP crusts, enriched in goethite have smaller amounts of these trace elements since these trace metals are associated with the Mn phase. The distribution of strategic elements reflects the mineralogy of crusts, as discussed below.

5.5.1. Fe, Mn and Co

Fe-oxyhydroxides and Mn-oxides are the most abundant minerals in the CISP crusts, as reflected in XRD and petrographic studies, the Fe minerals being greater than the Mn minerals. These minerals control the distribution of metals. Fe in Canary crusts essentially relies on the presence of feroxyhyte, an amorphous iron oxyhydroxide that with time collapses to more stable phases like goethite (Varentsov et al., 1991; Hein et al., 2000; Muiños et al., 2013). Fe shows a strong positive correlation with Mn (0.87) and negative correlation (from −0.5 to −0.7) with Mg, Al, K and Si. The correlation of Fe and Mn reflects the main crust mineralogy; both are siderophile elements with ionic radii of < 15% difference, which allows isomorphic replacement in the Fe-Mn oxyhydroxide minerals (Goldschmidt, 1937; Goldschmidt et al., 1954).

In contrast to Pacific crusts, Mn is depleted by about at least 30% (Table 3). The most important Mn mineral in the CISP Fe-Mn crusts is vernadite (δ-MnO_2). Mn and Fe have positive correlation with the same elements, particularly REEs, V, Mo, Pb, As and W. Fe has a stronger positive correlation with REEs than Mn, probably due to the major abundance of Fe in the structures of goethite-type minerals and Fe-vernadite. Zn has a positive correlation with Mn (0.8) and a weaker correlation with Fe (0.56) indicating that this metal dominantly associated with Mn oxide. The enrichment of Ni, Cu and Zn in CISP crusts affected by phosphatization and/or authigenic phyllosilicates (DR7-8; DR9-10; DR14-1) can be explained by the presence of todorokite and the absorption of these metals into the tunnel structure of this 10 Å manganate (Burns and Burns, 1978; Koschinsky et al., 1997; Hein et al., 2016). Ni and Cu exhibit a strong positive correlation (0.86) and with Si, Al and Mg (from 0.55 to 0.9), and no correlation with other metals, especially those linked to hydrogenesis (e.g., Co, Ce, V, Pb, As). This may indicate that these elements are associated with the phyllosilicates and manganates formed by authigenic processes, as observed on DRX studies.

Co is enriched in Fe-Mn crusts due to its entering the vernadite structure (Halbach et al., 1981, 1983; Baturin, 1988; Hein et al., 1997, 2000, 2013; Rona, 2008). This enrichment depends essentially on the substitution and adsorption that occurs directly on the surface of crusts. Co^{2+} dissolved in marine waters is oxidized to its trivalent phase Co^{3+}, which is less soluble. The CISP crusts with high Co contents show low growth rates (e.g., contents of 0.4 wt% have a growth rate of 2.7 mm/Ma while 0.7 wt% has growth rate of 1.2 mm/Ma). Nevertheless, Co shows a positive correlation with Mn and Fe; in the CISP crusts with coefficients of 0.58 and 0.55 (Supplementary Table 1). Co shows the strongest positive correlations with As (0.7) and Ce (0.61), and with other metals: Mo, Zn, V, Tl and LREEs (0.54–0.61). Positive correlations of Co with Mn and lower correlation with Fe in bulk samples indicate the presence of this element predominantly in the structure of Fe-vernadite.

5.5.2. REY and PGEs

REY are enriched in the CISP crusts (Table 3 and Fig. 8A and B). These elements are strategic for their use in hi-tech applications and in the manufacture of superconductors and super-magnets (Hein et al., 2013).

Pearson coefficients (Supplementary Table 1) show strong positive correlations among the REEs (>0.7) and with Fe (from 0.68 to 0.97). Mn has a weaker positive correlation with REEs (from 0.59 to 0.85). These correlation data reflect the strong affiliation of REY predominantly with Fe-oxyhydroxides and secondarily with Mn oxides. Correlations between REY and alumina-silicate elements are absent or negative (from −0.2 to −0.8), indicating only trace amounts of REY in the silicate minerals. REY have strong positive correlations with other metals presents in Fe-Mn crusts: As, V, Pb, Mo and W. All these trace metals are hosted in the Fe and Mn phases.

High contents of Ce in the CISP crusts (Fig. 8A and B) are typical of hydrogenetic deposits as well as strong positive Ce anomalies (Hein et al., 1988; Bau and Koschinsky, 2009). According to these authors, Ce enrichment in crusts depends on a preferential fractionation to the Fe and Mn phases, with a slight relative preference for Fe oxyhydroxides. The results provided by these authors indicate that the transfer of Ce from seawater does not occur via a discrete solid Ce (IV) oxide phase from dissolved Ce (III), but rather Ce dissolved in waters remains trivalent and its oxidation to the tetravalent form occurs at the surface of Fe-Mn oxyhydroxides after its sorption into their structure. Other tetravalent elements like Pt (IV), Zr (IV), Hf (IV) and Th (IV) instead react with Fe-Mn crusts and prefer Fe oxide phases. This is consistent with the results obtained in this study. Fe-Mn crusts from the Canary seamounts exhibit a higher enrichment in Ce and similar trivalent REY than similar deposits from all the oceans, due to the high abundance of Fe-rich minerals.

The degree of enrichment of REY is also related to the genetic model and crust growth rates (Bau and Koschinsky, 2009). Hydrogenesis via very slow growth rates (1–2 mm/Ma) allows REY to accumulate in Fe-Mn oxyhydroxide structures on crust surfaces. According to Sholkovitz et al. (1992) and Moffett (1990), this enrichment is strongly dependent on the time in which Fe-Mn minerals are in contact with seawater, therefore supporting the control of growth rates. De Carlo (1991) also suggested that the difference between LREEs and HREEs reflects changes in crust mineralogy and also that the Ce anomaly may reflect paleo-redox conditions in which the amount of trivalent ions increases. The CISP crusts show enrichment in LREEs (Fig. 8D and Table 3).

Discussion on the origin, occurrence and concentration of PGEs in Fe-Mn crusts is a hot topic and is the subject of many papers because of its economic importance for high-tech industries (Hein et al., 1988, 2010; Baturin et al., 2005; Banakar et al., 2007; Astakhova, 2008). According to many studies (Baturin, 1988; Halbach et al., 1989a, 1989b), PGEs enter into the Mn-oxide structure by co-precipitation due to oxidation on the δ-MnO_2 surfaces. Other authors proposed that Pt is sorbed from seawater and oxidized on FeO(OH) surfaces (Hein et al., 2003, 2005; Koschinsky et al., 2005). Platinum inorganic complexes, platinum hydroxo-chloro (II) and (IV) complexes, and organic complexes could exist as dissolved species in seawaters with typical pH values (Kubrakova et al., 2010). These complexes react with freshly precipitated Fe-Mn oxyhydroxides, reaching an adsorption percentage of 80% for organic complexes and up to 99% for inorganic platinum complexes (II), but over longer periods of time (Kubrakova et al., 2010). With time and the slow growth rates of hydrogenetic crusts, PGEs are enriched by several orders of magnitude over their concentrations in continental crust. Pt enrichment in Fe-Mn crusts may also be related to phosphatization, as proposed by Halbach et al. (1989a, 1989b). In the CISP crusts, a variable behaviour of Pt is observed in relation to phosphatization. One phosphatized crust is enriched in Pt (222 ng/g; DR7-8) compared to the average value for phosphatized crusts (184 ng/g) and the non-phosphatized crusts with less enrichment (182 ng/g). The most likely mechanism for CISP crusts is that Pt is adsorbed from seawater and then oxidized on the surface of the FeO(OH), as reflected by the high

Pt contents (222–321 ng/g) in crusts that are rich in Fe (DR2-9; DR13-12; DR15-14A). This mechanism of Pt enrichment is proposed for other crusts in the Atlantic, Indian and Pacific oceans (Hein et al., 2003; Banakar et al., 2007; Muiños et al., 2013). Pd is enriched in the CISP crusts in comparison with others from the Atlantic (Muiños et al., 2013) and Indian Oceans (Banakar et al., 2007). Banakar et al. (2007) proposed a cosmogenic origin for this element, by comparing the Pd/Ir ratio of several reservoirs and concluding that this ratio for Indian Fe-Mn crusts is similar to the value obtained in chondritic reservoirs (ranging from 0.7 to 2). The same ratio obtained in CISP samples yield the same range of values for all Fe-Mn crusts, with one from the Tropic Seamount reaching a Pd/Ir ratio similar to that of oceanic basalt (46).

6. Conclusions

We analyzed for the first time a complete suite of marine Fe-Mn deposits that were discovered in the southern Canary Island Seamount Province (CISP) in the northeastern tropical Atlantic. Fe-Mn crusts from Cretaceous seamounts (The Paps, Tropic, Echo and Drago) in CISP grow on their basalt-sedimentary substrate below the northeastern tropical Atlantic core of OMZ, reaching a maximum thickness up to 250 mm at depths of 2400 m on Drago seamount.

An important regime of upwelling currents near CISP supported a high biological productivity and consequently a more extensive OMZ, perhaps favoring the slow growth (1–2 mm/Ma) of Fe-Mn crusts on the slopes and summits of the seamounts.

Fe minerals are the most abundant. Mn phases are represented essentially by vernadite and minor quantities of todorokite and asbolane-buserite, all of which are intergrown with Fe oxyhydroxides. The high Fe enrichment in CISP crusts is due to upwelling of deep current ventilation and fertilization of the OMZ, Sahara dust, submarine volcanic plumes of CISP hotspot volcanoes over millions of years, and fluvial inputs to the Atlantic, which favored crusts with Fe/Mn ratios >1. Genetic models based on geochemical data confirm a hydrogenetic precipitation of the crusts. Phosphatization events are present in some crusts, especially in lower layers. The participation of hydrothermal fluids has not been identified from bulk crust geochemistry, however, future layer-by-layer EPMA composition of crusts will identify possible geochemical-mineralogical proxies of hydrothermal input.

Fe-Mn crusts from CISP shown high strategic metal average concentrations: Co (0.5%), Ni (0.3%), V (0.24%) and Ba (0.34%). REY reach high contents in CISP Fe-Mn crusts (total REY up to 0.35%) that are essentially enriched in LREEs and MREEs. Concentrations of REY strictly depend on crust mineralogy and especially on the abundance of Fe-oxyhydroxides. PGEs are enriched with the highest values for Pt (up to 321 ppb), Rh (up to 22 ppb), Ru (up to 19 ppb), and an anomalous crust with a high content of Pd (170 ppb). Early diagenesis and phosphatization promote the enrichment in Ni, Cu and PGEs. Although these crusts have relatively low contents of Ni (0.28%), Cu (0.07%) and Mn (16%) compared to Pacific crusts, they possess high concentrations of other critical metals such as REY (0.28%), V (0.24%) and Nb (0.01%).

Crusts were dated using a combination bulk crust geochemistry and high-resolution data along an EPMA transect, applied to a Co-chronometer. The age model allowed us to relate the different events of mineralization to tectonic and paleoceanographic events over the last 28 Ma:

1. An early growth period consisting of dense laminae, characterized by similar contents of Fe and Mn located at the interval between 27.8 and 24.45 Ma (late Oligocene-early Miocene) interpreted as slow precipitation in or below an extensive OMZ.

2. An intermediate, well-layered zone showing higher contents of Fe, Si and P in the interval between ca. 24.5 and 16 Ma shows high growth rates reaching 4.5 mm/Ma and the precipitation of Fe-Mn oxides promoted by the upwelling of deep currents and ventilation of the OMZ. The upper zone characterized by an abrupt increase in Fe at circa 16 Ma is interpreted to be the result of the incursion of the Northern Component Waters.

3. An uppermost zone with very low growth rates (to 0.5 mm/Ma) at circa 12 Ma to present, which is interpreted as the result of the increase in the extent of the OMZ in the NE Atlantic and the presence of a stable thermohaline circulation.

The Co-chronometer-determined growth rates and derived ages for bulk samples opens the possibility to investigate palaeoenvironmental changes that occurred over the last 76 Ma if the estimated ages are verified using Os isotope stratigraphy. Future detailed geochemical, chronological and isotopic analyses through the Fe-Mn crusts will provide useful information about the paleoenvironments that existed in the area throughout the Cenozoic.

Supplementary data to this article can be found online at http://dx.doi.org/10.1016/j.oregeorev.2016.10.005.

Acknowledgements

This work was supported by the Spanish projects SUBVENT (CGL2012-39524-C02), the Extension of the Continental Shelf of Spain project (CTM2010-09496-E), IGME project REMIMARES (IGME-2571) and European project EMODnet-Geology (2012/S96-158476). Egidio Marino also would like to thank the Ministry of Education, Culture and Sport its FPU scholarship (FPU014/06774).

The authors thank Captain Luis Gago and all the scientists and technical staff who participated in the oceanographic cruise DRAGO onboard the R/V Miguel Oliver, for data acquisition and for their expertise in collecting samples. We also thank the staff of "Centro Nacional de Microscopía Electrónica" and Laboratories of Crystallography and Mineralogy Department, Geology Faculty, both at the Complutense University of Madrid (UCM), and the Laboratories of the Geological Survey of Spain (IGME) for allowing us to use their facilities.

We thank Márta Polgári, Bramley Murton, an anonymous reviewer and helpful discussion with J.R. Hein and Editors for comments that helped improve this paper.

References

Abed, A.M., Al Kuisi, M., Khair, H.A., 2009. Characterization of the Khamaseen (spring) dust in Jordan. Atmos. Environ. 43, 2868–2876.

Abouchami, W., Galer, S.J.G., Koschinsky, A., 1999. Pb and Nd isotopes in NE Atlantic Fe–Mn crusts: proxies for trace metal paleosources and paleocean circulation. Geochim. Cosmochim. Acta 63 (10), 1489–1505.

Adachi, G.-Y., Imanaka, N., Tamura, S., 2010. Research trends in rare earths: a preliminary analysis. J. Rare Earths 28 (6):843–846. http://dx.doi.org/10.1016/S1002-0721(09)60207-6.

Ancochea, E., 2004. Evolución de la actividad volcánica. In: Vera, J.A. (Ed.), Geología de España. SGE-IGME, Madrid, pp. 639–641.

Anders, E., Ebihara, M., 1982. Solar-system abundances of the elements. Geochim. Cosmochim. Acta 46, 2363–2380.

Aparicio-González, A., Duarte, C.M., Tovar-Sánchez, A., 2012. Trace metals in deep ocean waters: A review. J. Mar. Syst. 100–101, 26–33.

Astakhova, N.V., 2008. Noble, rare earth, and nonferrous metals in ferromanganese cruses from submarine volcanoes of the sea of Japan. Dokl. Earth Sci. 422 (1), 1161–1166.

Banakar, V.K., Hein, J.R., 2000. Growth response of a deep-water ferromanganese crust to evolution of the Neogene Indian Ocean. Mar. Geol. 162, 529–540.

Banakar, V.K., Pattan, J.N., Mudholkar, A.V., 1997. Palaeoceanographic conditions during the formation of a ferromanganese crust from the Afanasiy-Nikitin seamount, North Central Indian Ocean: geochemical evidence. Mar. Geol. 136, 299–315.

Banakar, V.K., Hein, J.R., Rajani, R.P., Chodankar, A.R., 2007. Platinum group elements and gold in ferromanganese crusts from Afanasiy-Nikitin seamount, equatorial Indian Ocean: Sources and fractionation. Journal of Earth System Science 116 (1):3–13. http://dx.doi.org/10.1007/s12040-007-0002-x.

Bashmachnikov, I., Nascimento, Â., Neves, F., Menezes, T., Koldunov, N.V., 2015. Distribution of intermediate water masses in the subtropical northeast Atlantic. Ocean Sci. 11, 803–827.

Baturin, G.N., 1988. The Geochemistry of Manganese and Manganese Nodules in the Ocean. Springer, Netherlands.

Baturin, G.N., Dubinchuk, V.T., 2011. Mineralogy and chemistry of ferromanganese crusts from the Atlantic Ocean. Geochem. Int. 49 (6), 578–593.

Baturin, G.N., Konopleva, E.V., Dubinchuk, V.T., Mel'nikov, M.E., 2005. Platinum and gold in the ferromanganese crusts of the Pacific Ocean. Oceanology 45 (2), 269–276 (Engl. Transl.).

Baturin, G.N., Dubinchuk, V.T., Rashidov, V.A., 2012. Ferromanganese crusts from the sea of Okhotsk. Oceanology 52 (1):88–100. http://dx.doi.org/10.1134/S0001437012010031.

Bau, M., Koschinsky, A., 2009. Oxidative scavenging of cerium on hydrous Fe oxide: Evidence from the distribution of rare earth elements and yttrium between Fe oxides and Mn oxides in hydrogenetic ferromanganese crusts. Geochem. J. 43 (1):37–47. http://dx.doi.org/10.2343/geochemj.1.0005.

Bau, M., Schmidt, K., Koschinsky, A., Hein, J., Kuhn, T., Usui, A., 2014. Discriminating between different genetic types of marine ferro-manganese crusts and nodules based on rare earth elements and yttrium. Chem. Geol. 381:1–9. http://dx.doi.org/10.1016/j.chemgeo.2014.05.004.

Becerril, L., Cappello, A., Galindo, I., Neri, M., Del Negro, C., 2013. Spatial probability distribution of future volcanic eruptions at El Hierro Island (Canary Islands, Spain). J. Volcanol. Geotherm. Res. 257, 21–30.

Becerril, L., Galindo, I., Martí, J., Gudmundsson, A., 2015. Three-armed rifts or masked radial pattern of eruptive fissures? The intriguing case of El Hierro Volcano (Canary Islands). Tectonophysics 647–648, 33–47.

Bogdanov, Y.A., Sorochtin, O.G., Zonenshain, L.P., Kuptzov, V.M., Lisitzina, N.A., Podrajanski, A.M., 1990. Ferromanganese Crust and Nodules of Pacific Seamounts: Moscow (Nauka) (in Russian).

Bogdanov, Y.A., Bogdanova, O.Y., Dubinin, A.V., Gorand, A., Gorshkov, A.I., Gurvich, E.G., Isaeva, A.B., Ivanov, G.V., Jansa, L.F., Monaco, A., 1995. Composition of ferromanganese crusts and nodules at northwest Pacific guyots and geologic and paleoceanographic considerations. In: Haggerty, J.A., Premoli Silva, I., Rack, F.R., McNutt, M.K. (Eds.), Proceedings of the Ocean Drilling Program: Scientific Results. 144, p. 1059 (Ocean Drilling Program (College Station, TX)).

Bonatti, E., Kraemer, T., Rydell, H., 1972. Classification and genesis of submarine iron-manganese deposits. In: Horn, D.R. (Ed.), Ferromanganese Deposits of the Ocean Floor. Arden House, New York, pp. 149–165.

Brandt, P., Hormann, V., Körtzinger, A., Visbeck, M., Krahmann, G., Stramma, L., Lumpkin, R., Schmid, C., 2010. Changes in the ventilation of the oxygen minimum zone of the tropical North Atlantic. J. Phys. Oceanogr. 40:1784–1801. http://dx.doi.org/10.1175/2010JPO4301.1.

Brandt, P., Greatbatch, R.J., Claus, M., Didwischus, S.-H., Hormann, V., Funk, A., Hahn, J., Krahmann, G., Fischer, J., Körtzinger, A., 2012. Ventilation of the equatorial Atlantic by the equatorial deep jets. Journal of Geophysical Research: Oceans 117, C12015. http://dx.doi.org/10.1029/2012JC008118.

Burns, V.M., Burns, R.G., 1978. Post-depositional metal enrichment processes inside manganese nodules from the north equatorial Pacific. Earth Planet. Sci. Lett. 39 (3): 341–348. http://dx.doi.org/10.1016/0012-821X(78)90020-1.

Canet, C., Prol-Ledesma, R.M., Bandy, W.L., Schaaf, P., Linares, C., Camprubí, A., Tauler, E., Mortera-Gutiérrez, C., 2008. Mineralogical and geochemical constraints on the origin of ferromanganese crusts from the Rivera Plate (western margin of Mexico). Mar. Geol. 251, 47–59.

Carracedo, J.C., Pérez-Torrado, F.J., Ancochea, E., Meco, J., Hernán, F., Cubas, C.R., Casillas, R., Rodríguez Badiola, E., Ahijado, A., 2002. Cenozoic volcanism II: the Canary Islands. In: Gibbons, E., Moreno, M.T. (Eds.), The Geology of Spain. Geological Society, London, pp. 439–472.

Castillo, S., Moreno, T., Querol, X., Alastuey, A.s., Cuevas, E., Herrmann, L., Mounkaila, M., Gibbons, W., 2008. Trace element variation in size-fractionated African desert dusts. J. Arid Environ. 72 (6):1034–1045. http://dx.doi.org/10.1016/j.jaridenv.2007.12.007.

Condie, K.C., 1993. Chemical composition and evolution of the upper continental crust: contrasting results from surface samples and shales. Chem. Geol. 104:1–37. http://dx.doi.org/10.1016/0009-2541(93)90140-E.

Conrad, T., Hein, J.R., Paytan, A., Clague, D.A., 2017. Formation of Fe-Mn crusts within a continental margin environment. Ore Geol. Rev. 87, 25–40.

De Carlo, E.H., 1991. Paleoceanographic implication of rare earth element variability in a marine Fe-Mn crust from the Hawaiian Archipelago. Mar. Geol. 98, 449–467.

Delaney, P.T., Pollard, D.D., Ziony, I., Mckee, E.H., 1986. Field relations between dikes and joints: emplacement processes and paleostress analysis. 91, 4920–4938.

Ding, X., Gao, L., Fang, N.Q., Qu, W.J., Liu, J., Li, J., 2009. The relationship between the growth process of the ferromanganese crusts in the Pacific seamount and Cenozoic ocean evolvement. China Series D: Earth Sciences]–>Sci. China Ser. D Earth Sci. 52 (8), 1091–1103.

Donoghue, E., Troll, V.R., Harris, C., O'Halloran, A., Walter, T.R., Pérez Torrado, F.J., 2008. Low-temperature hydrothermal alteration of intra-caldera tuffs, Miocene Tejeda caldera, Gran Canaria, Canary Islands. J. Volcanol. Geotherm. Res. 176 (4), 551–564.

Dubinin, A.V., Rozanov, A.G., 2001. Geochemistry of rare earth elements and thorium in sediments and ferromanganese nodules of the Atlantic Ocean. Lithol. Miner. Resour. 36 (3):268–279. http://dx.doi.org/10.1023/A:1010485510346.

Dymond, J., Lyle, M., Finney, B., Piper, D.Z., Murphy, K., Conard, R., Pisias, N., 1984. Ferromanganese nodules from MANOP Sites H, S and R—control of mineralogical and chemical composition by multiple accretionary processes. Geochim. Cosmochim. Acta 48, 931–950.

Eltayeb, M.A.H., Injuk, J., Maenhaut, W., Van Grieken, R.E., 2001. Elemental Composition of mineral aerosol generated from Sudan Sahara Sand. J. Atmos. Chem. 40 (3), 247–273.

European Commission, 2016. http://ec.europa.eu/index_en.htm.

Formenti, P., Caquineau, S., Desboeufs, K., Klaver, A., Chevaillier, S., Journet, E., Rajot, J.L., 2014. Mapping the physico-chemical properties of mineral dust in western Africa: mineralogical composition. Atmos. Chem. Phys. 14 (19):10663–10686. http://dx.doi.org/10.5194/acp-14-10663-2014.

Glasby, G.P., Mountain, B., Vineesh, T.C., Banakar, V., Rajani, R., Ren, X., 2010. Role of hydrology in the formation of Co-rich Mn crusts from the equatorial N Pacific, equatorial S Indian Ocean and the NE Atlantic Ocean. Resour. Geol. 60 (2), 165–177.

Goldschmidt, V.M., 1937. The principles of distribution of chemical elements in minerals and rocks. The seventh Hugo Muller Lecture, delivered before the Chemical Society on March 17th, 1937. J. Chem. Soc.:655–673 http://dx.doi.org/10.1039/JR9370000655 ((Resumed)(0)).

Goldschmidt, V.M., Muir, A., University of O, 1954. Geochemistry. Clarendon press, Oxford.

González, F.J. 2011. Geochemical Study of Undersea Volcanic Plume Emission From El Hierro Island, Canary Islands. (Unpublished Report).

González, F.J., Somoza, L., León, R., Medialdea, T., de Torres, T., Ortiz, J.E., Lunar, R., Martínez-frías, J., Merinero, R., 2012. Ferromanganese nodules and micro-hardgrounds associated with the Cadiz Contourite Channel (NE Atlantic): palaeoenvironmental records of fluid venting and bottom currents. Chem. Geol. 310–311:56–78. http://dx.doi.org/10.1016/j.chemgeo.2012.03.030.

González, F.J., Somoza, L., Medialdea, T., León, R., Vázquez, J.T., Marino, E., Bellido, E., Reyes, J., 2014a. Volcanism and ferromanganese deposits on seamounts and new volcanoes from the Canary Archipelago. IV Congress of Marine Sciences, At Las Palmas de Gran Canaria, Spain, Volume: Book of Abstracts Submitted to the IV Congress of Marine Sciences. 186 (ISBN-10: 84-697-0471-0; ISBN-13: 978-84-697-0471-4).

González, F.J., Somoza, L., Lunar, R., Martínez-Frías, J., Medialdea, T., León, R., Martín-Rubí, J.A., Torres, T., Ortiz, J.E., Marino, E., 2014b. Polymetallic ferromanganese deposits research on the Atlantic Spanish continental margin. In: Hein, J.R., Barriga, F.J.A.S., Morgan, C.L. (Eds.), 43rd Underwater Mining Institute Conference (Lisbon).

González, F.J., Somoza, L., Hein, J.R., Medialdea, T., León, R., Urgorri, V., Reyes, J., Martín-Rubí, J.A., 2016. Phosphorites, Co-rich Mn nodules, and Fe-Mn crusts from Galicia Bank, NE Atlantic: reflections of Cenozoic tectonics and paleoceanography. Geochem. Geophys. Geosyst. 17. http://dx.doi.org/10.1002/2015GC005861.

Grousset, F.E., Biscaye, P.E., 2005. Tracing dust sources and transport patterns using Sr, Nd and Pb isotopes. Chem. Geol. 222, 149–167.

Grousset, F.E., Parra, M., Bory, A., Martinez, P., Bertrand, P., Shimmield, G., Ellam, R.M., 1998. Saharan wind regimes traced by the Sr-Nd isotopic composition of subtropical Atlantic sediments: last glacial maximum vs today. Quat. Sci. Rev. 17 (4–5), 395–409.

Halbach, P., Hebisch, U., Scherhag, C., 1981. Geochemical variations of ferromanganese nodules and crusts from different provinces of the Pacific Ocean and their genetic control. Chem. Geol. 34 (1):3–17. http://dx.doi.org/10.1016/0009-2541(81)90067-X.

Halbach, P., Segl, M., Puteanus, D., Mangini, A., 1983. Co-fluxes and growth rates in ferromanganese deposits from central Pacific seamount areas. Nature 304 (5928), 716–719.

Halbach, P., Kriete, C., Prause, B., Puteanus, D., 1989a. Mechanisms to explain the platinum concentration in ferromanganese seamount crusts. Chem. Geol. 76 (1):95–106. http://dx.doi.org/10.1016/0009-2541(89)90130-7.

Halbach, P., Sattler, C.-D., Teichmann, F., Wahsner, M., 1989b. Cobalt-rich and platinum bearing manganese crust deposits on seamounts: nature, formation, and metal potential. Mar. Min. 8, 23–39.

Hannington, M.D., Petersen, S., Santana-Casiano, M., Fraile-Nuez, E., Klischies, M., Lange, S., Hissman, K., Schauer, J., Striewski, P., Anderson, M.O., Nicolai, M., van Rouveroy, M., 2016. POS-494 Leg 2 Cruise Report: Assessment of Ongoing Magmatic-hydrothermal Discharge of the El Hierro Submarine Volcano, Canary Islands, by the Submersible JAGO. Cruise report POS494-2. p. 88.

Hatta, M., Measures, C.I., Wu, J., Roshan, S., Fitzsimmons, J.N., Sedwick, P., Morton, P., 2015. An overview of dissolved Fe and Mn distributions during the 2010–2011 U.S. GEOTRACES north Atlantic cruises: GEOTRACES GA03. Deep-Sea Res. II Top. Stud. Oceanogr. 116:117–129. http://dx.doi.org/10.1016/j.dsr2.2014.07.005.

Hein, J.R., 2004. Cobalt-rich ferromanganese crusts. Global distribution, composition, origin and research activities. Minerals Other Than Polymetallic Nodules of the International Seabed Area, Chapter: 5. International Seabed Authority, pp. 188–256.

Hein, J.R., Koschinsky, A., 2014. 13.11 — deep-ocean ferromanganese crusts and nodules. In: Turekian, H.D.H.K. (Ed.), Treatise on Geochemistry, second edition Elsevier, Oxford, pp. 273–291.

Hein, J.R., Morgan, C.L., 1999. Influence of substrate rocks on Fe-Mn crust composition. Deep-sea Research Part I: Oceanographic Research Papers 46 (5):855–875. http://dx.doi.org/10.1016/S0967-0637(98)00097-1.

Hein, J.R., Petersen, S., 2013. The geology of sea-floor massive sulphides. In: Baker, E., Beaudoin, Y. (Eds.), Deep Sea Minerals: Sea-Floor Massive Sulphides, a Physical, Biological, Environmental, and Technical Review 1A. Secretariat of the Pacific Community.

Hein, J.R., Schwab, W.C., Davis, A., 1988. Cobalt- and platinum-rich ferromanganese crusts and associated substrate rocks from the Marshall Islands. Mar. Geol. 78 (3–4): 255–283. http://dx.doi.org/10.1016/0025-3227(88)90113-2.

Hein, J.R., Schulz, M.S., Kang, J.-K., 1990. Insular and submarine ferromanganese mineralization of the Tonga-Lau region. Mar. Min. 9 (3), 305–354.

Hein, J.R., Yeh, H.-W., Gunn, S.H., Sliter, W.V., Benninger, L.M., Wang, C.-H., 1993. Two major Cenozoic episodes of phosphogenesis recorded in equatorial Pacific seamount deposits. Paleoceanography 8 (2), 293–311.

Hein, J.R., Koschinsky, A., Halbach, P., Manheim, F.T., Bau, M., Kang, J.K., Lubick, N., 1997. Iron and manganese oxide mineralization in the Pacific. Geol. Soc. Spec. Publ. 119, 123–138.

Hein, J.R., Koschinsky, A., Bau, M., Manheim, F.T., Kang, J.K., Roberts, L., 2000. Co-rich ferromanganese crusts in the Pacific. In: Cronan, D.S. (Ed.), Handbook of Marine Mineral Deposits. CRC Marine Science Series. CRC Press, Boca Raton, Florida, pp. 239–279.

Hein, J.R., Koschinsky, A., Halliday, A.N., 2003. Global occurrence of tellurium-rich ferromanganese crusts and a model for the enrichment of tellurium. Geochim. Cosmochim. Acta 67 (6):1117–1127. http://dx.doi.org/10.1016/S0016-7037(02)01279-6.

Hein, J.R., McIntyre, B., Koschinsky, A., 2005. The global enrichment of platinum group elements in marine ferromanganese crusts. In: Törmänen, T.O., Alapieti, T.T. (Eds.), Extended Abstracts, 10th International Platinum Symposium, pp. 98–101 (Oulu, Finland).

Hein, J.R., Conrad, T.A., Staudigel, H., 2010. Seamount mineral deposits: a source of rare metals for high technology industries. Oceanography 23 (1), 184–189.

Hein, J.R., Mizell, K., Koschinsky, A., Conrad, T.A., 2013. Deep-ocean mineral deposits as a source of critical metals for high- and green-technology applications: comparison

with land-based resources. Ore Geol. Rev. 51:1–14. http://dx.doi.org/10.1016/j.oregeorev.2012.12.001.
Hein, J.R., Spinardi, F., Okamoto, N., Mizell, K., Thorburn, D., Tawake, A., 2015. Critical metals in manganese nodules from the CookIslands EEZ, abundances and distributions. Ore Geol. Rev. 68, 97–116.
Hein, J.R., Conrad, T., Mizell, K., Banakar, V.K., Frey, F.A., Sager, W.W., 2016. Controls on ferromanganese crust composition and reconnaissance resource potential, Ninetyeast Ridge, Indian Ocean. Deep-Sea Research I 110:1–19. http://dx.doi.org/10.1016/j.dsr.2015.11.006.
Helmers, E., Schrems, O., 1995. Wet deposition of metals to the tropical North and the South Atlantic ocean. Atmos. Environ. 29 (18), 2475–2484.
Henderiks, J., 2001. Coccolith Studies in the Canary Basin: Glacial-interglacial Paleoceanography of the Eastern Boundary Current System. Unpubl. PhD thesis. 14086. ETH Zürich, Switzerland (175 pp.).
Hernández-Guerra, A., Fraile-Nuez, E., López-Laatzen, F., Martínez, A., Parrilla, G., Vélez-Belchí, P., 2005. Canary current and north equatorial current from an inverse box model. J. Geophys. Res. 110, C12019. http://dx.doi.org/10.1029/2005JC003032.
IGME, Instituto Geológico y Minero de España. (2015). Presentación parcial de datos e información sobre los límites de la Plataforma Continental de España al Oeste de las Islas Canarias, conforme a la Parte VI y el Anexo II de la Convención de las Naciones Unidas sobre el Derecho del Mar. 5 Vols. (Unpublished).
ISBA, 2016. International Seabed Authority. https://www.isa.org.jm.
Jackson, S.E., Fryer, B.J., Gosse, W., Healey, D.C., Longerich, H.P., Strong, D.F., 1990. Determination of the precious metals in geological materials by inductively coupled plasma-mass spectrometry (ICP-MS) with nickel sulphide fire-assay collection and tellurium coprecipitation. Chem. Geol. 83 (1–2):119–132. http://dx.doi.org/10.1016/0009-2541(90)90144-V.
Kandler, K., Schütz, L., Jäckel, S., Lieke, K., Emmel, C., Müller-Ebert, D., Ebert, M., Scheuvens, D., Schladitz, A., Šegvić, B., Wiedensohler, A., Weinbruch, S., 2011. Ground-based off-line aerosol measurements at Praia, Cape Verde, during the Saharan Mineral Dust Experiment: microphysical properties and mineralogy. Tellus: Series B 63 (4), 459–474.
Knoll, M., Hernández-Guerra, A., Lenz, B., López Laatzen, F., Machín, F., Müller, T.J., Siedler, G., 2002. The Eastern Boundary Current system between the Canary Islands and the African Coast. Deep-Sea Res. II Top. Stud. Oceanogr. 49 (17):3427–3440. http://dx.doi.org/10.1016/S0967-0645(02)00105-4.
Koschinsky, A., Hein, J.R., 2003. Uptake of elements from seawater by ferromanganese crusts: solid-phase associations and seawater speciation. Mar. Geol. 198 (3–4): 331–351. http://dx.doi.org/10.1016/S0025-3227(03)00122-1.
Koschinsky, A., van Gerven, M., Halbach, P., 1995. First discovery and investigation of massive ferromanganese crusts in the NE Atlantic in comparison to hydrogenetic Pacific occurrences. Mar. Georesour. Geotechnol. 13, 375–391.
Koschinsky, A., Halbach, P., Hein, J.R., Mangini, A., 1996. Ferromanganese crusts as indicators for paleoceanographic events in the NE Atlantic. Geol. Rundsch. 85 (3):567–576. http://dx.doi.org/10.1007/BF02369011.
Koschinsky, A., Stascheit, A., Bau, M., Halbach, P., 1997. Effects of phosphatization on the geochemical and mineralogical composition of marine ferromanganese crusts. Geochim. Cosmochim. Acta 61, 4079–4094.
Koschinsky, A., Audroing, J., Hein, J.R., 2005. The enrichment of platinum and fractionation of Pt from Pd in marine ferromanganese crusts. In: Törmänen, T.O., Alapieti, T.T. (Eds.), Extended Abstracts, 10th International Platinum Symposium, pp. 429–432 (Oulu, Finland).
Kröepelin, S., 2006. Revisiting the age of the Sahara desert. Science 312 (5777): 1138–1139. http://dx.doi.org/10.1126/science.312.5777.1138b.
Kubrakova, I.V., Koshcheeva, I.Y., Tyutyunnik, O.A., Asavin, A.M., 2010. Role of organic matter in the accumulation of platinum in oceanic ferromanganese deposits. Geochem. Int. 48 (7):655–663. http://dx.doi.org/10.1134/S0016702910070037.
Lázaro, F.J., Gutiérrez, L., Barrón, V., Gelado, M.D., 2008. The speciation of iron in desert dust collected in Gran Canaria (Canary Islands): combined chemical, magnetic and optical analysis. Atmos. Environ. 42, 8987–8996.
Li, Z., Feng, Y., 2006. Determination of the platinum group elements in geological samples by ICP-MS after NiS fire assay and Te coprecipitation: ultrasound-assisted extraction of PGEs from Te precipitate. J. Anal. At. Spectrom. 21 (1):90–93. http://dx.doi.org/10.1039/B511763A.
Lindblom, S., Gérard, M., 1998. Textural and fluid inclusion evidence for hydrothermal activity in the volcaniclastic apron of Gran Canaria. Proceedings of the Ocean Drilling Program, Scientific Results. 157, pp. 429–439.
Lyle, M., 1981. Formation and growth of ferromanganese oxides on the Nazca plate. In: al., L.D.K.e. (Ed.), Nazca Plate: Crustal Formation and Andean Convergence. 154, pp. 269–293 Geol. Soc. Am. Mem.
Machín, F., Hernández-Guerra, A., Pelegrí, J.L., 2006. Mass fluxes in the Canary Basin. Prog. Oceanogr. 70 (2–4):416–447. http://dx.doi.org/10.1016/j.pocean.2006.03.019.
Maldonado, A., Bohoyo, F., Galindo-Zaldívar, J., Hernández-Molina, F.J., Lobo, F.J., Lodolo, E., Martos, Y.M., Pérez, L.F., Schreider, A.A., Somoza, L., 2014. A model of oceanic development by ridge jumping: opening of the Scotia Sea. Glob. Planet. Chang. 123 (Part B):152–173. http://dx.doi.org/10.1016/j.gloplacha.2014.06.010.
Manheim, F.T., Lane-Bostwick, C.M., 1988. Cobalt in ferromanganese crusts as a monitor of hydrothermal discharge on the Pacific sea floor. Nature 335 (6185), 59–62.
Marino, E., González, F.J., Lunar, R., Somoza, L., Bellido, E., Castillo Carrión, M., Reyes, J., 2014. Las costras de hierro-manganeso de los montes submarinos canarios como fuente de metales estratégicos y de tierras raras. Macla 19.
Massari, S., Ruberti, M., 2013. Rare earth elements as critical raw materials: focus on international markets and future strategies. Res. Policy 38 (1):36–43. http://dx.doi.org/10.1016/j.resourpol. 2012.07.001.
Melnikov, M.E., Pletnev, S.P., 2013. Age and formation conditions of the Co-rich manganese crust on guyots of the Magellan seamounts. Lithol. Miner. Resour. 48 (1), 1–13.
Mémery, L., Arhan, M., Alvarez-Salgado, X.A., Messias, M.-J., Mercier, H., Castro, C.G., Rios, A.F., 2000. The water masses along the western boundary of the south and equatorial Atlantic. Prog. Oceanogr. 47, 69–98.
Mendez, J., Guieu, C., Adkins, J., 2010. Atmospheric input of manganese and iron to the ocean: seawater dissolution experiments with Saharan and North American dusts. Mar. Chem. 120, 34–43.
Milne, A., Landing, W., Bizimis, M., Morton, P., 2010. Determination of Mn, Fe, Co, Ni, Cu, Zn, Cd and Pb in seawater using high resolution magnetic sector inductively coupled mass spectrometry (HR-ICP-MS). Anal. Chim. Acta 665, 200–207.
Moffett, J.W., 1990. Microbially mediated cerium oxidation in sea water. Nature 345 (6274), 421–423.
Moreno, T., Querol, X., Castillo, S., Alastuey, A., Cuevas, E., Herrmann, L., Mounkaila, M., Elvira, J., Gibbons, W., 2006. Geochemical variations in eolian mineral particles from the Sahara — Sahel Dust Corridor. Chemosphere 65 (2), 261–270.
Muhs, D.R., Budahn, J., Skipp, G., Prospero, J.M., Patterson, D., Bettis Iii, E.A., 2010. Geochemical and mineralogical evidence for Sahara and Sahel dust additions to quaternary soils on Lanzarote, eastern Canary Islands, Spain. Terra Nova 22 (6), 399–410.
Muiños, S.B., Hein, J.R., Frank, M., Monteiro, J.H., Gaspar, L., Conrad, T., Pereira, H.G., Abrantes, F., 2013. Deep-sea Fe-Mn crusts from the northeast Atlantic Ocean: composition and resource considerations. Mar. Georesour. Geotechnol. 31 (1):40–70. http://dx.doi.org/10.1080/1064119X.2012.661215.
Müller-Michaelis, A., Uenzelmann-Neben, G., Stein, R., 2013. A revised Early Miocene age for the instigation of the Eirik Drift, offshore southern Greenland: evidence from high-resolution seismic reflection data. Mar. Geol. 340, 1–15.
Murray, J., Renard, A.F., 1891. Manganese Deposits From the HMS Challenger Stations Supplement to: Murray, John; Renard, A F (1891): Deep-sea Deposits (Based on the Specimens Collected During the Voyage of HMS Challenger in the Years 1872 to 1876). Report on the Scientific Results of the Voyage of H.M.S. Challenger During the Years 1873–76. John Menzies and Co., Endinburgh, United Kingdom orignal link. http://www.vliz.be/nl/open-marien-archief?module=ref&refid=41584 (688 pp (pdf 252 Mb), hdl:10013/epic.45942.d002: PANGAEA).
Newman, H.R., 2011. The mineral industries of Morocco and Western Sahara U.S. Geological Survey Minerals Yearbook V. III 10 pp.
Nielsen, S.G., Mar-Gerrison, S., Gannoun, A., LaRowe, D., Klemm, V., Halliday, A.N., Burton, K.W., and Hein, J.R., 2009. Thallium isotope evidence for a permanent increase in marine organic carbon export in the early Eocene. Earth Planet. Sci. Lett., v. 278, p. 297–307.
Palomino, D., Vázquez, J.-T., Somoza, L., León, R., López-González, N., Medialdea, T., Fernández-Salas, L.-M., González, F.-J., Rengel, J.A., 2016. Geomorphological features in the southern Canary Island volcanic province: the importance of volcanic processes and massive slope instabilities associated with seamounts. Geomorphology 255, 125–139.
Pastor, M.V., Vélez-Belchí, P., Hernández-Guerra, A., 2015. Water masses in the Canary current large marine ecosystem. In: Valdés, L., Déniz-González, I. (Eds.), Oceanographic and Biological Features in the Canary Current Large Marine Ecosystem. IOC-UNESCO, Paris. IOC Technical Series 115, pp. 73–79.
Paulmier, A., Ruiz-Pino, D., 2009. Oxygen minimum zones (OMZs) in the modern ocean. Progress in Oceanography 80 (3–4), 113–128.
Pohl, C., Croot, P.L., Hennings, U., Daberkow, T., Budeus, G., Loeff, M., Rutgers, v.d., 2011. Synoptic transects on the distribution of trace elements (Hg, Pb, Cd, Cu, Ni, Zn, Co, Mn, Fe, and Al) in surface waters of the Northern- and Southern East Atlantic. J. Mar. Syst. 84 (1–2), 28–41.
Puteanus, D., Halbach, P., 1988. Correlation of Co concentration and growth rate — a method for age determination of ferromanganese crusts. Chem. Geol. 69 (1–2): 73–85. http://dx.doi.org/10.1016/0009-2541(88)90159-3.
Rajani, R.P., Banakar, V.K., Parthiban, G., Mudholkar, A.V., Chodankar, A.R., 2005. Compositional variation and genesis of ferromanganese crusts of the Afanasiy–Nikitin Seamount, Equatorial Indian Ocean. Journal of Earth System Science 114, 51–61.
Reyss, J.L., Marchig, V., Ku, T.L., 1982. Rapid growth of a deep-sea manganese nodule. Nature 295 (5848), 401–403.
Rodríguez-Losada, J.A., Martinez-Frias, J., Bustillo, M.A., Delgado, A., Hernandez-Pacheco, A., de la Fuente Krauss, J.V., 2000. The hydrothermally altered ankaramite basalts of Punta Poyata (Tenerife, Canary Islands). J. Volcanol. Geotherm. Res. 103, 367–376.
Rona, P.A., 2008. The changing vision of marine minerals. Ore Geol. Rev. 33 (3–4): 618–666. http://dx.doi.org/10.1016/j.oregeorev.2007.03.006.
Saager, P.M., de Baar, H.J.W., de Jong, J.T.M., Nolting, R.F., Schijf, J., 1997. Hydrography and local sources of dissolved trace metals Mn, Ni, Cu, and Cd in the northeast Atlantic Ocean. Mar. Chem. 57, 195–216.
Santana-Casiano, J.M., González-Dávila, M., Fraile-Nuez, E., de Armas, D., González, A.G., Domínguez-Yanes, J.F., Escánez, J., 2013. The natural ocean acidification and fertilization event caused by the submarine eruption of El Hierro. Sci. Report. 3, 1–8.
Santana-Casiano, J.M., Fraile-Nuez, E., González-Dávila, M., Baker, E.T., Resing, J.A., Walker, S.L., 2016. Significant discharge of CO2 from hydrothermalism associated with the submarine volcano of El Hierro Island. Sci. Report. 6:25686. http://dx.doi.org/10.1038/srep25686.
Sarnthein, M., Thiede, J., Pflaumann, U., Erlenkeuser, H., Fiitterer, D., Koopmann, B., Lange, H., Seibold, E., 1982. Atmospheric and oceanic circulation patterns off northwest Africa during the past 25 million years. In: von Rad, U., Hinz, K., Sarnthein, M., Seibold, E. (Eds.), Geology of Northwest Africa Continental Margin. Springer-Verlag, Berlin Heidelberg-New York, pp. 545–604.
Scheuvens, D., Schütz, L., Kandler, K., Ebert, M., Weinbruch, S., 2013. Bulk composition of northern African dust and its source sediments — a compilation. Earth Sci. Rev. 116: 170–194. http://dx.doi.org/10.1016/j.earscirev. 2012.08.005.
Schiffman, P., Staudigel, H., 1994. Hydrothermal alteration of a seamount complex on La Palma, Canary Islands: implications for metamorphism in accreted terranes. Geology 22, 151–154.

Schmincke, H.-U., Krastel, S., Hansteen, T., Sumita, M., H.-U., G., G., 2000. Preliminary results, Leg M43/1, rock sampling and description. DECOS/OMEX II, Cruise No. 43, 25 November 1998–14 January 1999. METEOR-Berichte, Hamburg, p. 99.

Schuster, M., Duringer, P., Ghienne, J.-F., Vignaud, P., Mackaye, H.T., Likius, A., Brunet, M., 2006. The age of the Sahara Desert. Science 311 (5762) (821 pp.).

Sepulchre, P., Ramstein, G., Fluteau, F., Schuster, M., Tiercelin, J.-J., Brunet, M., 2006. Tectonic uplift and Eastern Africa aridification. Science 313 (5792), 1419–1423.

Sholkovitz, E.R., Shaw, T.J., Schneider, D.L., 1992. The geochemistry of rare earth elements in the seasonally anoxic water column and porewaters of Chesapeake Bay. Geochim. Cosmochim. Acta 56 (9):3389–3402. http://dx.doi.org/10.1016/0016-7037(92)90386-W.

Sincell, M., 1999. A wobbly start for the Sahara. Science 285 (5426) (325 pp.).

Somoza, L., and SUBVENT Scientific Party. 2014. SUBVENT II Report cruise. (Unpublished report).

Somoza, L., Vázquez, J.T., González-Aller, D., Dañobeitia, J.J., Medialdea, T., Moya, A.J., Fernández-Salas, L.M., León, R., Jurado, M.J., Paredes, M., Palomino, D., Vargas, I., González, F.J., López-Rodríguez, M., Corbalán, A., González, P., Hernández-Puentes, M.P., Martín-Jiménez, D., 2012. Geophysical and hydroacoustic study of the active submarine volcanism in the El Hierro Island (Canarian Archipelago). Geotemas 13, 601–605.

Somoza, L., González, F.J., Madureira, P., Barker, S.J., Medialdea, T., de Ignacio, C., Lourenço, N., León, R., Vazquez, J.T., 2016. Evolution of submarine eruptive activity during the 2011–2012 El Hierro event as documented by hydroacoustic images and remotely operated vehicle observations. Geochem. Geophys. Geosyst. (Submitted).

Stoker, M.S., Hoult, R.J., Nielsen, T., Hjelstuen, B.O., Laberg, J.S., Shannon, P.M., Praeg, D., Mathiesen, A., van Weering, T.C.E., McDonnell, A., 2005. Sedimentary and oceanographic responses to early Neogene compression on the NW European margin. Mar. Pet. Geol. 22:1031–1044. http://dx.doi.org/10.1016/j.marpetgeo.2005.01.009.

Swezey, C., 1999. A very old Sahara. Science 286 (5438) (239 pp.).

Taylor, S.R., McLennan, S.M., 1985. The Continental Crust; Its Composition and Evolution; an Examination of the Geochemical Record Preserved in Sedimentary Rocks. 312. Blackwell, Oxford.

Usui, A., Nishi, K., Sato, H., Thornton, B., Kashiwabara, T., Tokumaru, A., Sakaguchi, A., Yamoaka, K., Kato, S., Nitahara, S., Suzuki, K., Ijima, K., Urabe, T., 2017. Continuous growth of hydrogenetic ferromanganese crusts since 17 Myr ago on Takuyo-Daigo Seamount, NW Pacific, at water depths from 800–5500 m. Ore Geol. Rev. 87, 71–87.

van den Bogaard, P., 2013. The origin of the Canary Island Seamount Province — New Ages of Old Seamounts. Scientific Reports. 3:p. 2107. http://dx.doi.org/10.1038/srep02107. http://www.nature.com/articles/srep02107#supplementary-information.

Varentsov, I.M., Drits, V.A., Gorshkov, A.I., Sivtsov, A.V., Sakharov, B.A., 1991. Mn-Fe oxyhydroxide crusts from Krylov Seamount (Eastern Atlantic): mineralogy, geochemistry and genesis. Mar. Geol. 96 (1):53–70. http://dx.doi.org/10.1016/0025-3227(91)90201-E.

Wang, G., Jansa, L., Chu, F., Zou, C., Sun, G., 2015. Composition and origin of ferromanganese crusts from equatorial western Pacific seamounts. China]–>J. Ocean Univ. China 14 (2), 217–227.

Wedepohl, K.H., 1991. Chemical-composition and fractionation of the continental-crust. Geol. Rundsch. 80 (2), 207–223.

Wedepohl, K.H., 1995. The composition of the continental crust. Geochim. Cosmochim. Acta 59 (7):1217–1232. http://dx.doi.org/10.1016/0016-7037(95)00038-2.

Wegorzewski, A.V., Kuhn, T., Dohrmann, R., Wirth, R., Grangeon, S., 2015. Mineralogical characterization of individual growth structures of Mn-nodules with different Ni + Cu content from the central Pacific Ocean. Am. Mineral. 100, 2497–2508.

Whiteley, J.D., Murray, F., 2005. Determination of platinum group elements (PGE) in environmental samples by ICP-MS: a critical assessment of matrix separation for the mitigation of interferences. Geochemistry: Exploration, Environment, Analysis 5 (1):3–10. http://dx.doi.org/10.1144/1467-7873/03-035.

Zhang, Z., Ramstein, G., Schuster, M., Li, C., Contoux, C., Yan, Q., 2014. Aridification of the Sahara desert caused by Tethys Sea shrinkage during the Late Miocene. Nature 513 (7518), 401–404.